REMOTE OPTICAL SENSING AND QUANTIFICATION OF SINGLE ANALYTE MOLECULES IN LIQUIDS THROUGH A WAVEGUIDE

INAUGURALDISSERTATION

zur
Erlangung der Würde eines Doktors der Philosophie
vorgelegt der
Philosophisch-Naturwissenschaftlichen Fakultät
der Universität Basel

von

Philippe Haas
aus Luzern und Kriens, Luzern

Basel 2006

Genehmigt von der Philosophisch-Naturwissenschaftlichen Fakultät

auf Antrag von

Prof. Dr. sc. nat. Hans-Joachim Güntherodt
Prof. Dr. phil. II Bert Hecht
PD Dr. sc. nat. Martin Hegner

Basel, den 2. Mai 2006

Prof. Dr. sc. techn. Hans-Jakob Wirz
Dekan

For my wife, Natalia

Table of Contents

1. Summary

In the work at hand a novel method to detect and quantify single oligonucleotide molecules in liquids is introduced. The aim consists of rapid specific quantification of mRNA molecules in solutions at room temperature by applying free-floating fluorescent molecular switches as integral part of an optical biosensor. The implementation of molecular switches enables the sensor to specifically detect unlabelled oligonucleotide sequences. In the thesis the crucial components consisting of the detection algorithm, the optical setup and the molecular switches (molecular beacons) are elaborated.

In order to be able to detect single fluorescent bursts in solutions the necessary software has to be developed. Herefore a method for the unambiguous detection of transient burst-like signals in presence of significant stationary noise is described. In order to discriminate a transient signal from the background noise an optimum threshold is determined using an iterative algorithm that isolates the probability distribution of the background noise. Knowledge of the probability distribution of the noise allows excluding the detection of false positive events with a defined probability. The method can be applied to the detection of transient single-molecule fluorescence events in presence of a strong background.

Using this peak detection method the sensing of single oligo-FRET molecules in buffer solution through a cleaved single mode optical fiber is demonstrated. Both the excitation light and the fluorescence signal are coupled through the same fiber thus implementing a remote detection scheme. The background luminescence created in the glass fiber by the strong excitation light is largely suppressed by the use of a wavelength-shifting concept. Fluorescence bursts are observed by proper stirring of the test solution. In addition, a discussion of the detection efficiency of the cleaved fiber by means of dipole radiation patterns near the glass/water interface is offered.

In a next step the optimal operation conditions of the setup are described and investigated by varying the relevant parameters over a wide range. This indicates the optimum values for the stirring velocity, the excitation intensity, the bin width and the experiment duration.

In the next step single molecule detection of oligonucleotide FRET constructs in liquids through a single-mode fiber is applied using the optimal detection conditions, which only then allows for quantification of ultra-low concentrations. A linear dependence of the number of detected fluorescence bursts on the concentration of the test solution over a wide dynamic range is demonstrated, starting at pM down to 1aM concentrations. This qualifies the algorithm and the apparatus to be applied in quantitative sensing applications and establishes the software and hardware elements as a functional unity.

Finally the molecular switches are implicated into the system. The application of molecular beacons to specific detection and quantification of characteristic mRNA sequences in a test solution is demonstrated. In bulk experiments, the performance of the molecular beacons is checked. It is found that single base pair mismatches between beacon and target sequence can be detected through the analysis of melting curves. Single-molecule experiments performed using the optical setup with molecular beacons in absence of targets show that only a negligible fraction of beacons is open at room temperature and produce fluorescence bursts. Upon addition of perfect targets the number of detected bursts increases dramatically. A linear dependence of the number of fluorescence bursts as a function of the concentration of molecular beacon-target sequence duplexes is observed. Furthermore, for a fixed concentration of molecular beacons, a linear increase of the number of bursts as a function of the target sequence concentration can be observed.

2. Introduction

The search for molecular markers that predict the prognosis of individual patients or the response to a gene specific treatment is a major focus in medical but especially in cancer research [1-4]. During the last years, much progress has been made in this field. Trastuzumab (Herceptin®) for blocking of HER2 receptor mediated tumor growth in metastasic breast cancer has become a paradigm for the feasibility of targeted therapy [5-10]. Imatinib (Glivec®), targeting the Kit-receptor has shown to be effective in both chronic myeloic leukemia [11-13] and gastrointestinal stroma tumors [14-16], indicating that targeted therapy is not necessarily limited to a single cancer type. The identification of specific gene expression profiles that predict response to docetaxel (Taxotere®) treatment in breast cancer, or the finding of EGF receptor mutations predicting response to gefitinib (Iressa®) treatment in lung cancer, marks another milestone in the development of new therapeutic regimens [17-20]. It can be expected that numerous additional molecular markers will be identified for a variety of different neoplasias. But molecular markers are not only of interest to cancer researchers and certainly not limited to neoplasias. Recent results in ophthalmological research for instance show that lymphocytes in the blood respond to glaucoma or glaucomatous damage with a clear difference in gene expression [21-23].

These two apparently completely different medical research areas exemplify the trend in medical research and outline not only the interdisciplinary field of molecular medicine for the entire medical sciences but accentuate the importance of interdisciplinary collaboration between physics, biology and medicine. One could argue that this junction of disciplines is a little far fetched but it truly represents the spirit of the “nanoscale sciences”. This is mandatory if molecular processes are to be thoroughly understood. As diseases mostly start at a cellular, not to say molecular level, it certainly represents the scale of interest for future diagnostic and therapy procedures [24-27].

The development outlined above prompts for the investigation of reliable and sensitive tests for the detection and quantification of therapy target genes and their gene products. To date, suitable diagnostic methods include detection of DNA copy numbers (e.g. by fluorescence in situ hybridization (FISH) [28-31], quantitative polymerase chain reaction (PCR), Southern blotting) [32-33], RNA expression (real-time PCR (RT-PCR), RNA in situ hybridization, Northern blotting) [34-35] or protein levels (immunohistochemistry (IHC), Western blotting) [36-37]. Such techniques are still to this day time consuming, expensive, and require extensive pretreatment of the samples [38]. If the disadvantages of an IHC based protein detection assay shall be avoided, it becomes necessary to develop easy to use tools for routine quantification of mRNA levels, especially considering that currently used methods to determine the genetic status of tissues may take one to two weeks in specialized centers [39]. In addition, these assays have only limited capabilities for the real-time parallel investigation of multiple markers. Yet they do share one common factor: they all eventually rely on fluorescence as information carrier.

Fluorescence is a powerful tool for detection and quantification of molecules. During the last 10 years there has been a rapid development of optical microscopy [40-41]. Today single fluorescent molecules can be detected routinely in various environments ranging from liquids over polymers to living cells [42-46]. The ultimate sensitivity of detecting a single fluorescent molecule is due to the extreme specificity of fluorescence. The absorption cross-section for fluorescence processes is 11 orders of magnitude larger than the cross sections of competing methods that also generate red-shifted light [47]. This means that it is possible to detect a single fluorescent molecule in the presence of 10^{10} environmental molecules [48]. Such numbers can be easily reached by sufficiently reducing the effective illuminated volume [47,49,51]. The detection of single molecules in solution turns out to be not so much an issue of sensitive detection as of background reduction. Experimental schemes that overcome background noise problems but still have the ability to detect and quantify low concentrations will

suit the need for modern medical molecular diagnostics perfectly. What remains to be considered are the overall demands for a tool able to perform in this field.
An optimal diagnostic tool should allow for parallel investigation of multiple markers at the bedside or even in situ, with only minimal invasiveness but maximal sensitivity and specificity. In order to properly assess a possible genetic amplification or deletion it has to be able to rapidly quantify the target of interest within a sample solution. Preparation of the sample for an examination should require minimum time and manpower efforts. This implicates a minimum of sample pretreatment procedures, such as filtering, centrifugation, PCR, adsorption to an interface or labeling of the target molecules and consecutive rinsing of the sample. Simultaneously such a tool should remain universally applicable to any molecular detection and quantification task, irrelevant to the specific target molecule of interest. Most suitably reusable, it should consist of a fixed hardware component and of a disposable part, preferably remotely located.

These guidelines have lead to following approach described in Figure 1. Molecular switches are inserted into a sample solution. As long as the switch has not bound to any specific target it will almost yield no fluorescence signal, even if the fluorophore of the switch is properly excited by the laser beam of the sensor. Only if its specific target is present in the solution, the switch will bind to the target. The so generated complex consisting of molecular switch and target will force a conformational change of the original molecular switch structure, which is then translated into an altered fluorescent property of the duplex structure. The change of the fluorescence behavior of a molecular switch that has bound to its target is so significant that it can be easily discriminated from the ever-present background noise [50]. It should be emphasized that the here proposed method does not resort to any previous adsorption or immobilization procedures of the molecular switches to some sort of sensor interface, for instance an optical transducer, or comparable elements. The molecular switches remain completely free-floating within the sample solution.

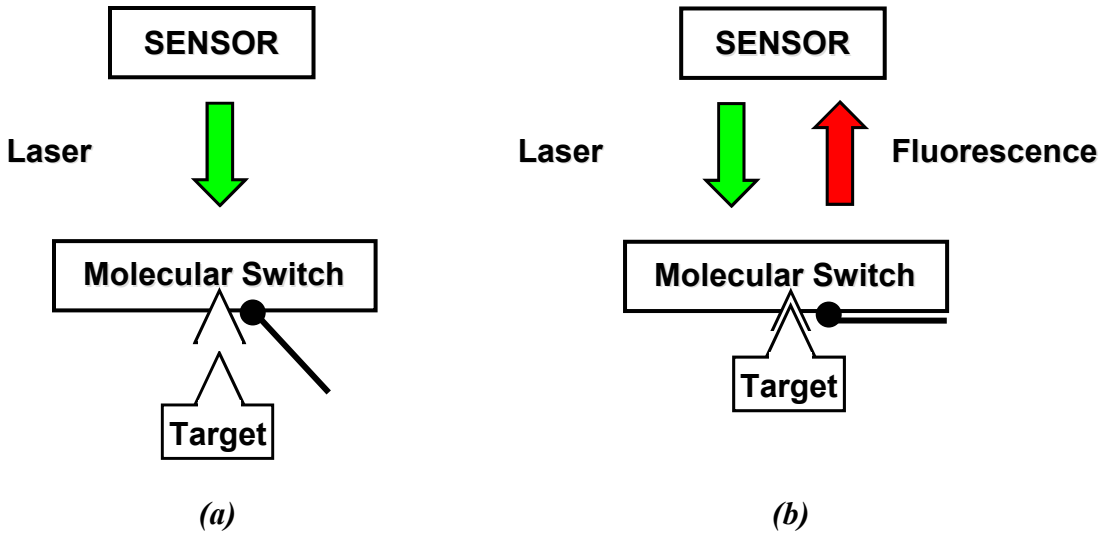

Figure 1: demonstrates the core idea of the here-proposed method. The sensor component excites via its laser the fluorophores of the free-floating molecular switch. A fluorescent signal is only then detected by the sensor, if the switch successfully bound to its specific target (b).

More detailed description of the function of the molecular switches (molecular beacons, smart probes) and their structure is provided in chapter five.

The goal of this thesis is to devise a simple, cheap and fast method that is able to quantify ultra-small concentrations of relevant molecular targets using an optical detection scheme based on fluorescence. In order to keep the setup simple but still having a built in potential for parallelization and lager-scale integration and miniaturization, it was decided to excite and detect single molecules through an optical waveguide. The use of an optical waveguide bears the tremendous advantage of being compatible with lab-on-the-chip platforms. Our approach provides the basis for the implementation of single-molecule detection assay in lab-on-the-chip architectures, which have the potential to completely outrange today's techniques in molecular diagnostics for the above-mentioned reasons. In the following the HER2 mRNA sequence shall serve as a model and will be used as target sequence throughout the thesis.

The thesis is a compilation of 4 publications to be submitted, including a description of the determination of optimal operation parameters, which elaborates on the steps necessary to achieve a successful combination of free-floating molecular switches and an optical biosensor. The outline is as follows:

The third chapter deals with the problem of detecting transient signals, like fluorescence bursts, in the presence of significant background noise. While it is the common opinion that single molecules can only be detected under extreme low noise conditions, it here is demonstrated that reliable counting of single fluorescence bursts in the presence of significant background noise accumulated in the optical waveguide can be achieved.

The fourth chapter introduces the optical setup used and discusses its principles of operation. A first qualitative proof of principle of the detection scheme is provided.
Hence the chapter addresses the question of optimal operation conditions for the setup. All relevant parameters are discussed and their optimal values are determined in experiments. Furthermore the chapter demonstrates that the setup may be used as an optical biosensor that is able to quantify the concentration of certain target molecules in a liquid. To this end a linear relationship between concentration and number of detected fluorescence bursts is demonstrated. A dynamic range of many orders of magnitude is visualized starting at pM concentrations going down to one aM.

Eventually, the fifth chapter proofs that the optical setup can be combined with highly specific molecular beacons that are able to detect the presence of target mRNA sequences. The detection of perfect mRNA targets in buffer is demonstrated. For a fixed concentration of free-floating molecular beacons the

concentration of targets can be monitored by determining the ratio of open to closed beacons.

Finally, after establishing this new detection and quantification method including the use of molecular switches the sixth chapter offers an outlook to future applications in body fluids. For this purpose a similar experiment as described in chapter five is performed, however by replacing the buffer solution with human blood. The results proof that the method at hand is also suitable to work in body fluids with residuals of corpuscular elements and that their autofluorescence properties do not interfere with the sensor's function.

References

1. Pecorino L., Molecular Biology of Cancer, 2005, *Oxford University Press*.
2. Koichi Nagasaki and Yoshio Miki, *Breast Cancer*, 2006, 13, 2-7.
3. Laura J. van 't Veer *et al.*, *Nature,* 2002, 415, 530-536.
4. van de Vijver MJ *et al.*, *N. Engl. J. Med.,* 2002, 347, 1999-2009.
5. Revillion, F. *et al.*, *Eur. J. Cancer,* 1998, 34, 791-808.
6. Wang S.C. *et al.*, *Semin. Oncol.,* 2001, 28 (Suppl. 18) 21-29.
7. Van't V. et al., *Nature*, 2002, 415, 530-535.
8. Press MF. et al., *Clin. Cancer Res.* 2005, 11(18), 6598-607.
9. Yeon C.H. et al., *Invest. New Drugs*., 2005, 23 (5), 391-409.
10. Dundachi N. et al., *Anticancer Res*., 2004, 24 (4), 2401-6.
11. Diana Lüftner *et al.*, *Clinical Biochemistry,* 2003, 36, 233-240.
12. Radich *et al.*, *Proc. Natl. Acad. Sci. USA*, 2006, 103, 2794-2799.
13. Druker B.J., *Trends Mol. Med*., 2002, 8, 14-18.
14. Francis J. *et al*., *Current Mol. Medicine*, 2005, 5, 615-623.
15. Went P.T. et al., *J. Clin. Oncol*., 2004, 22(22), 4514-22.
16. Capdeville R. et al., 2002, *Nature Rev. Drug Discovery*, 1, 493-502.
17. Hurley J. et al., *J. Clin. Oncol*. 2006, [Epub ahead of print].
18. Gordon B. Mills *et al*., *Rev. Clin. Exp. Hematol.*, 2003, 30 (Suppl. 16), 93-104.
19. Lynch T.J. et al., 2004, *N. Engl. J. Med*.,350, 2129-2139.
20. Paez J.G. et al., 2004, *Science*, 304, 1497-1500.
21. Golubnitschaja O. et al., *Curr. Eye Res.*, 2000; 5: 325-331
22. Golubnitschaja O. et al., *J. Glaucoma*, 2004; 13: 66-72
23. Flammer J. et al., *Prog. Retin. Eye Res.*, 2002; 21: 359-393
24. Moran N., *Nat. Biotechnol*. 2006, 2,121.
25. Brower V., J. *Natl. Cancer Inst*. 2006, 98 (1),9-11.

26. Shaffer C., *Drug Discov Today*. 2005, 10 (23-24),1581-2.
27. Li K.C., *Biomed. Microdevices*., 2004, 6 (2), 113-6.
28. Sauter G. et al., *Acta Cytol*., 1996, 40 (2),164-73.
29. Sauter G. et al., *Verh. Dtsch. Ges. Pathol*., 1993, 77, 247-51.
30. Zaharieva B. et al., *Int. J. Cancer*, 2005, 117 (6), 952-6.
31. Xin-Lin Mu *et al*., *BMC Cancer*, 2004, 4,51.
32. Yuan E. et al., *Cancer Res*., 2006, 66 (7), 3443-51.
33. Lebeau A *et al*., *J. Clin. Oncol.,* 2001, 19, 354-36.
34. Wilson C.A. et al., *Breast Cancer Res*. 2005, 7 (6), 1058-79.
35. Rosanna W. et al., *BMC Genomics*, 2005, 6, 180.
36. Lanteri M. et al., *Breast Cancer Res*. 2005, 7, 487-494.
37. Wilson C.A. et al., *Breast Cancer Res*., 2005, 7 (6), 1058-79.
38. Mansfield E.S. et al., *Mol. Cell Probes*, 1995, 9 (3), 145-56.
39. Petersen B.L., *Appl. Immunohistochem. Mol. Morphol*., 2004, 12 (3), 259-65.
40. Valeur B. et Bronchon J.C (Eds), New Trends in Fluorescence Spectroscopy, Applications to Chemical and Life Sciences, 2001, *Springer-Verlag,* Berlin.
41. Wolfbreis O.S. (Ed), Fluorescence Spectroscopy, New Methods and Applications, 1993, *Springer-Verlag*, Berlin.
42. Rigler R.J., *J. Biotechnol*., 1995, 41, 177-186.
43. Brinkmeier M. et al., *Biophys. Chem*., 1997, 66, 229-239.
44. Rigler R.J. et al., *Proc. SPIE*, 1992, 1921, 239-248.
45. Rigler R. J. et al., *Bioscience*, 1990, 3, 180-183.
46. Mets Ue. et al., *J. Fluoresc*., 1994, 4, 259-264.
47. Valeur B. (Ed), Molecular Fluorescence, Principles and Applications, 2002, *Wiley-VCH*.
48. Novotny L. and Hecht B., Principles of Nano-Optics, 2006, *Cambridge University Press.*

49. Machara M.P. et al., *Bioimaging*, 1998, 6, 33-42.
50. Feringa B. L., Molecular Switches, 2001, *Wiley-VCH*.
51. Zander Ch., Enderlein J., Keller R.A. (Eds), Single Molecule Detection in Solutions, 2002, *Wiley-VCH*.

3. Detection of transient events in the presence of background noise

3.1 Introduction

The detection of rare transient events (bursts) above a strong stationary background noise with a high level of confidence is a problem of broad interest in various sensing applications ranging from ultra-sensitive optical detection e.g. for biological assays or medical diagnostics, over electromagnetic sensors, to defence applications. In general, a transient signal is considered to be detected above the noise either if (i) its amplitude is many standard deviations above the mean value of the noise's probability distribution or if (ii) the wave form, i.e. the duration of the transient event is clearly distinct from the noise's characteristic fluctuations in time [1,2,3,4].

Here we propose a method which is applicable in particular if the signal bursts are neither easily distinguishable from the characteristic fluctuations of the noise nor their amplitude is large enough to be considered clearly above the noise. The method is based on a fast converging iterative algorithm, which determines an optimum threshold for the detection of bursts. It provides a quantitative measure for the probability of false positive events due to the background noise peaks, which may be predefined by the user. The reliability of the method is assessed by performing Monte-Carlo simulations of the burst detection process. To demonstrate the method's potential we detect and count single-molecule fluorescence bursts recorded in presence of a significant stationary background noise.

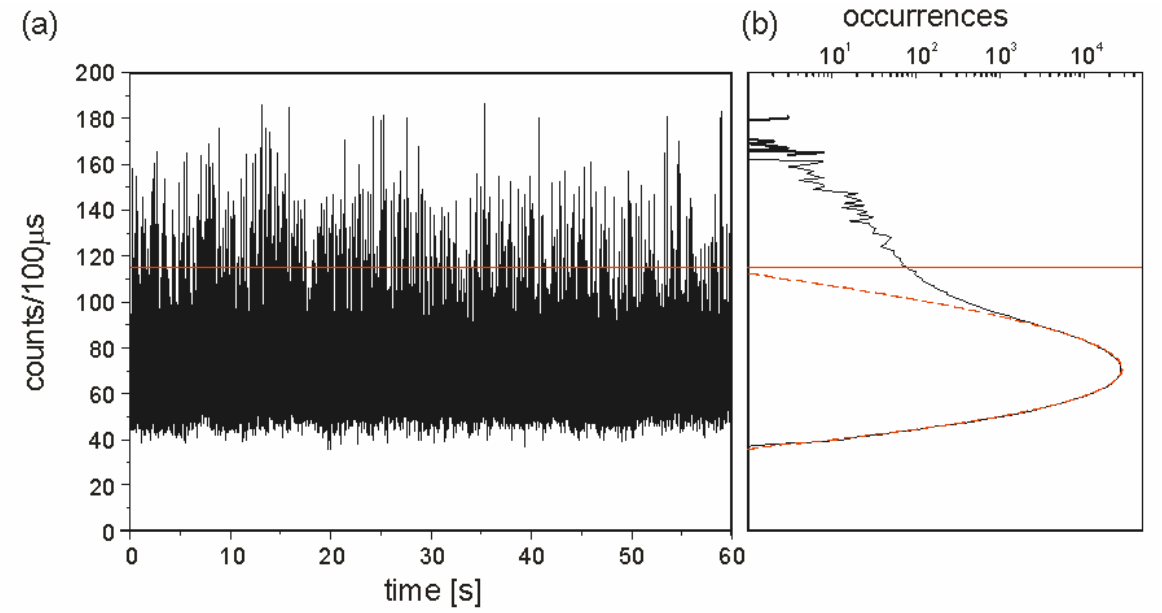

Figure 1: Time trace and histogram of a model data set. (a) Time trace with a bin width of 100 µs showing fluorescence bursts on top of a strong Poissonian background. (b) Histogram of the time trace in (a). The fluorescence bursts lead to a characteristic deviation from Poissonian statistics. The horizontal line shows the threshold level above which signals are counted as burst. The dashed curve plotted together with the histogram is the best estimate for the noise probability distribution obtained by calculating the mean of the noise after removing bursts above threshold (see text). A remarkably good agreement is obtained.

3.2 Algorithm

To simplify the discussion, but without loss of generality, we consider a data set describing a time series of counts per time interval containing rare transient events (bursts) in presence of a significant background noise with a Poissonian

distribution. The algorithm outlined in the following can be easily adapted to accommodate different types of stationary noise, e.g. Gaussian noise. Apart from being sufficiently rare, no further assumptions are made with respect to the amplitude and shape distribution of the transient events superimposed to the noise. Figure 1(a) shows a time trace of a typical experimentally obtained data set that serves as an example along side with the respective histogram *H(n)* (Figure 1(b)). Here *n* is the number of counts per 100 μs. Fluorescence bursts of various amplitudes are observed above the background noise. *H(n)* shows a clearly distinguishable main Poissonian noise peak and a tail that accounts for the fluorescence bursts. As can be seen in Figure 1(b) the number of transient events characterized by the respective area of the histogram is small compared to the area of the noise peak. We note that *H(n)* may be thought of as consisting of a sum of two separate histograms - one describing the pure background noise and one describing the distribution of signal bursts such that $H(n) = P(n) + S(n)$, where *P(n)* describes the distribution of background counts and *S(n)* describes the distribution of signal burst heights. Signal bursts cannot be easily separated from the noise since both distributions overlap. To optimally discriminate signal bursts from similar events due to background noise a threshold must be determined above which a burst is counted as a signal burst. The threshold must on the one hand be low enough in order to miss as few as possible true signal peaks and on the other hand it must be high enough to exclude the possibility to count a strong fluctuation of the noise as a signal. The latter would contribute to false positive events which in view of applications e.g. in medical diagnostics have to be minimized because of possible expensive consequences or even false treatment. To determine such an optimum threshold the probability distribution of the background, *P(n)*, in the present example the normalized Poissonian distribution characterized by its mean μ and the variance $\sigma = \sqrt{\mu}$

$$P(n) = \frac{e^{-\mu}\mu^{n}}{n!} \tag{1}$$

must be recovered from the data as precisely as possible. Assuming that this has been achieved, we may consider the probability distribution of the background alone. This enables us to determine a threshold for burst amplitude χ by demanding that the absolute number of time intervals *K* for which the number of counts *n* exceeds the threshold χ is smaller than a still tolerable small number, say e.g. 1. *K(χ)* is determined as

$$K(\chi) = N \times \left(1 - \int_{-\infty}^{\chi} P(n) dn \right) \tag{2}$$

where *N* is the total number of time intervals (bins) in the data set. We see that for $\chi \to \infty$, the number of false positive events *K(χ)* approaches zero, as expected. For a finite threshold χ, *K(χ)* is different from zero but can always be made sufficiently small by choosing the right value of χ. We may for example define the threshold $\hat{\chi}$ by the implicit equation

$$K(\hat{\chi}) \overset{!}{=} 1 \tag{3}$$

which corresponds to the detection of one false positive event in *N* data bins. Having reached this point, the problem of distinguishing a transient event from the background is reduced to the task of finding a sufficiently good estimate for the probability distribution of the background alone. To find such an estimate we propose using an iterative method. In a first iteration, the original data set is used to calculate an estimate for the mean, μ_1, and the standard deviation, σ_1, for the true μ and σ that characterize the noise. Since μ_1, σ_1 are calculated for the entire data set including peaks well above the noise, we expect that μ_1, σ_1 overestimate the true μ, σ. Assuming a Poisson distribution we fail - in this first iteration - to accurately fit the noise peak of the histogram *H(n)*. However we may still use μ_1 to obtain a first estimate for the noise distribution

$$P_1(n) = \frac{e^{-\mu_1} {\mu_1}^n}{n!} \tag{4}$$

which may then be used to calculate and estimate $K_1(\chi)$ *for the true* $K(\chi)$

$$K_1(\chi) = N \times \left(1 - \int_{-\infty}^{\chi} P_1(n) dn \right) . \quad (5)$$

Fig. 2 shows a plot of $K_1(\chi)$ together with

$$K_{ns}(\chi) = N \times \left(1 - \int_{-\infty}^{\chi} H(n) dn \right) \quad (6)$$

which is the analog of Eq. (2) however using the histogram $H(n) = P(n) + S(n)$ of the time trace of Fig. 1 (b) instead of $P(n)$ alone. Now $K_1(\chi)$ is used to calculated a first estimate $\hat{\chi}_1$ for the true value of $\hat{\chi}$ by invoking the analogue to Eq. (3) for $K_1(\chi)$. The respective solution of (3) is visualized in the zoom of $K_1(\chi)$ in Figure 2.

Once a first threshold $\hat{\chi}_1$ is determined, the next step consists in counting fluorescence burtsts with countrates above $\hat{\chi}_1$. This task is performed using a Labview (NI) routine based on an algorithm that fits a quadratic polynomial to a sequence of data points. The main inputs of the routine are the threshold $\hat{\chi}_1$ and the number of consecutive bins M to be used in the fit.

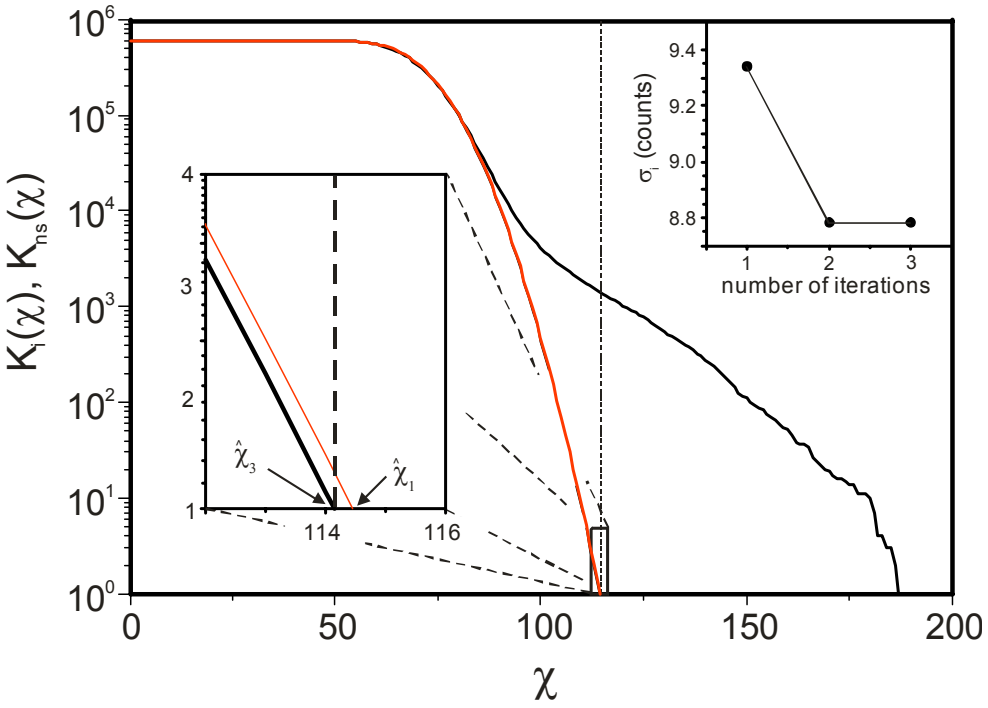

Figure 2: Visualization of $K_i(\chi)$. Already the first estimate of $K(\chi)$ obtained by calculating the mean of the time trace of Fig.1 provides a good estimate for the threshold. After three iterations all fluorescence bursts are eliminated. The mean of the remaining time trace perfectly characterizes the noise distribution.

Setting a small width *M* allows a finer resolution of the search for transient events but is prone to the detection of multiple peaks due to fluctuations on broader peaks. In contrary, a too large width prevents the detection of short bursts. To overcome the limitations of either situation, peak detection is performed as follows: the width is gradually decreased starting from a pre-defined maximum pixel number *M*. For each value of the width the number of detected bursts is stored. Each detected burst is then removed from the data by removing the respective bins. After *M* runs of the burst detection routine all bursts above $\hat{\chi}_1$ have been counted and removed. The remaining data set now consists of the background noise plus a few peaks with amplitudes smaller than $\hat{\chi}_1$. In the second iteration step the truncated data set obtained in the first iteration is used to calculate new estimates, μ_2 and σ_2 that better characterize the probability

distribution of the noise. As a consequence, more bursts are expected to be found in this second iteration step when applying the burst finding algorithm described before. After *i* iteration steps, μ_i (σ_i) converges to a stable minimum μ (σ), which then provides a very good estimate for the parameter describing the true histogram of the background noise *P(n)* (Eq. 1). In practice it is found that the algorithm converges extremely fast. As can be seen in the inset of Figure 2, the standard deviation of the truncated data set is stable already after 2 iterations. The zoom of $K(\chi)$ in Figure 2 shows that the final threshold $\hat{\chi}_3$ is only marginally smaller than the first estimate. The resulting best estimate for the noise distribution using the parameter μ_3 is plotted in Figure 1 together with histogram of the time trace. A remarkable agreement is found.

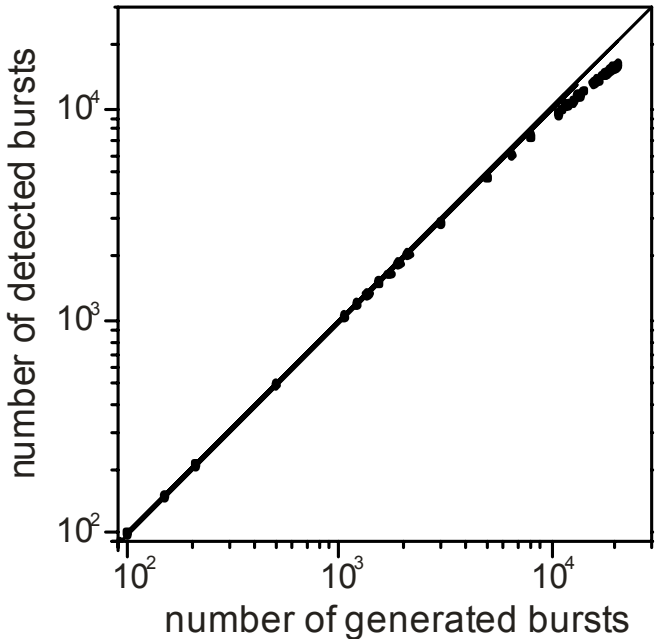

Figure 3: Monte-Carlo simulation of the burst detection process. The number of artificially generated bursts superimposed to a Poissonian noise is plotted against the number of bursts recovered by applying the burst detection algorithm. Bursts are faithfully recovered for burst densities up to several thousand bursts per trace. For higher burst densities significant overlap between bursts starts to diminuish the number of recovered bursts.

3.3 Discussion

Finally, we apply a Monte-Carlo simulation of the burst counting process to investigate the reliability of the proposed algorithm. To this end we generate artificial time traces consisting of Poissonian noise with superimposed bursts of a fixed amplitude that are randomly distributed in time. The number of superimposed bursts is varied to assess the performance of the algorithm at high densities of bursts. To each generated trace the burst detection algorithm as described above is applied and the number of detected bursts is plotted versus the actual number of bursts. The result is displayed in Figure 3. Obviously, the number of recovered bursts well recovered up to a several thousand bursts per trace. For larger numbers of bursts less bursts are recovered due to the onset of significant probability of overlap between bursts which are then counted as single event. We would like to stress the fact that the deviation observed is not a limitation of the presented algorithm but is a problem inherent to the type of data that are analysed. Monte-Carlo simulations can be used to determine correction factors to recover the actual number of bursts in applications that require very high precision and linearity.

3.4 Conclusion

We introduced an algorithm that is able to faithfully recover transient events in the presence of significant stationary noise. The method is based on the determination of an optimal detection threshold that avoids the detection of false positive events while recovering most of transient events. Using the proposed algorithm recovery of single-molecule fluorescence bursts in presence of a strong Poissonian background was demonstrated. The method presented here provides the basis for the analysis of single-molecule fluorescence burst data discussed in the following chapters.

3.5 References

1. Haab B.B. and Mathies, Anal. Chem., 1995, 67, 3253-3260.
2. Burns M.A. et al., Science, 1998, 282, 484-487.
3. Soper S.A. et al., Anal. Chem., 1993, 65, 740-747.
4. Ambrose W. P. et al., Chem. Rev., 1999, 99, 2929-2956.

4. Real-time remote detection and quantification of fluorescent wavelength-shifting oligonucleotides in liquids through an optical waveguide

4.1 Introduction

The detection and quantification of biomarkers is widely linked to the detection of fluorescence as described in chapter two. For techniques such as immunoassays, flow cytometry and chromatographic analysis the detection limits are from 10^3 to 10^6 fluorescent molecules [1], while automated DNA sequencing is limited to the range of 10^6 to 10^7 molecules and additionally requires PCR [2,3] for the amplification of the target amount. Fluorescence however holds the capacity for single-molecule detection in the attomolar range and even below [4-7]. This basically makes target amplification superfluous. During the past ten years, new fluorescence techniques have evolved capable of detecting single molecules in solutions [8-9]. Most of these methods however rely on the use of objectives [10-11]. The advantage of using integrated optics such as optical transducers instead of objectives would allow for miniaturization [14]. Unfortunately the current examples using waveguides are far from reaching single molecule detection. With the here-presented method it can be shown that it is possible to detect single molecules fluorescence through a waveguide. In addition, the ability of this method to be able to count free-floating molecules in a solution also renders the adsorption of molecules to an interface obsolete and therefore complicated chemical modification of surfaces can be avoided. Stirring of the sample solution is mandatory since within static liquids the fluorophore molecules in close proximity to the glass fiber would already be completely bleached before reaching the glass fiber core (see chapter 4.3.1).

The detection and quantification method will be described and tested on short fluorescent-labelled oligonucleotides that will serve as target molecules. This will

eliminate the switch-function, thus avoiding any possible confusion about the open or closed configuration of the switches and to assure that a target molecule will always emit a fluorescent signal when passing the detection volume of the glass fiber sensor. The aim of this chapter is, by applying the previously established algorithm, to successfully detect and quantify the oligonucleotide target molecules using the optical setup as described below.

4.2 Experimental

4.2.1 Experimental Optical Setup

A scheme of the setup is shown in Fig. 1. Excitation light **2** is provided by a He Ne laser (HeNe, λ=632.8 nm, max power 35 mW) **1.** A fiber aligner **5** (Fiber Positioner Kit, FS/S, New Focus) is used to couple the light into a single-mode fiber **3** (ClearLite 630-11,#cf042447, length ca. 0.4 m, Laser Components). The fiber should consist of a dielectric material of higher index than the test solution **S** which is the case for standard liquids and glass fibers. In the test solution, target molecules **T** of interest are excited by the light emitted at the vertically cleaved far fiber end causing the target molecules to emit fluorescence. The fluorescence of molecules that are sufficiently close to the fiber is coupled back into the fiber and is emitted at the other end. Here it is collimated by the microscope objective included in the fiber aligner. The beam of fluorescence passes a dichroic mirror **4** (XF3307 800WB80 17311, Omega Optical Inc., AR Coat R 633) and an optical filter **6** (T740/140 650 dcip, cube 38x26, Chroma Technology Corp.). The latter filter cuts of the excitation light and passes the fluorescence. The fluorescence is then focused (Achromat Lens, LAC896-B, Thorlabs Inc., USA) to the 200μm active area of a single-photon counting avalanche photodiode **8** (SPAD, Single Photon Counting Module; dark count rate < 250 c/s, SPCM-AQR-13, Perkin Elmer). The lens has a focal length of 200mm to ensure that the image of the fiber core on the SPAD is slightly smaller than the SPAD's active area. This avoids the detection of excess autofluorescence from the fiber cladding. Finally, the SPAD is read out by a computer equipped with a counter/timer board **9** (Labview 7.1, BNC 2120, NI Multifunction Board, NI PCI-6052E I/O, Shielded Connector BLK, SCB-68 BLK, National Instruments).

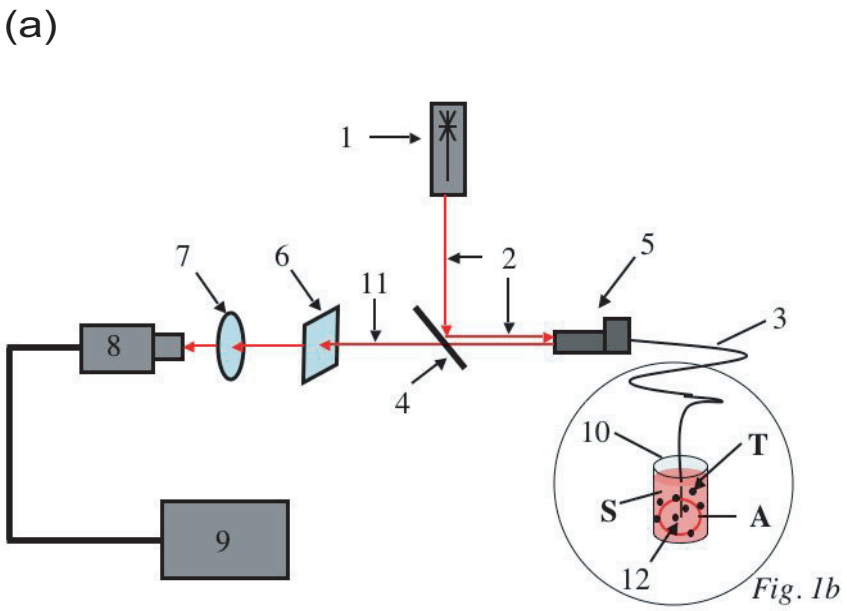

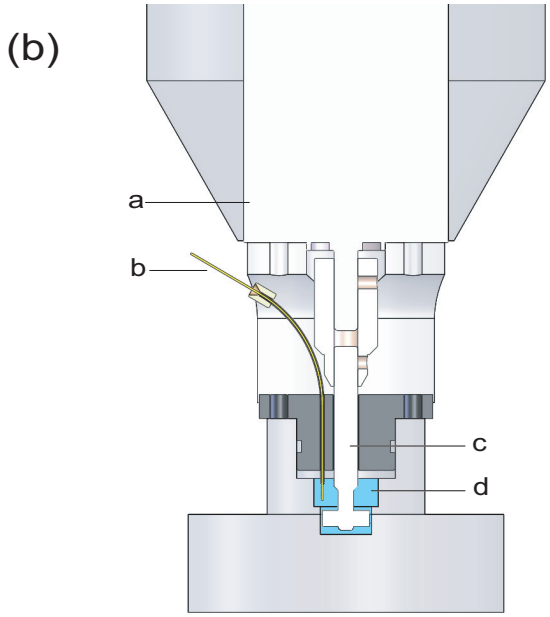

Figure 1(a): Experimental setup. A HeNe-Laser is coupled into a glass fiber via a dichroic mirror. At the end of the glass fiber, single fluorophore molecules are excited and couple a part of their fluorescent signal back into the fiber. The fluorescent signal passes the dichroic mirror, is filtered and is then focused onto a single photon counting module.

Figure 1(b): Motor (a), glass fiber (b), stirrer (c), fluid chamber (d)

A test solution containing target molecules of interest is prepared and presented in a self-designed PMMA fluid cell **10** able to contain up to 1.5 ml of test solution. An adjustable mechanical stirring device ensures proper initial homogenization of the solution and is then able to rotate with up to 25000 rpm. When in use, the freshly cleaved end of the optical fiber **3** (Miller Stripper Fo 103-S Oski, Fiber Cleaver S315, Furohawa, Mesomatic, Cham, Switzerland). is immersed about 1 cm in the solution **S**.

4.2.2 Basic Principles of Fluorescence

Typical fluorescence techniques rely upon the absorption of a photon by a fluorophore at one wavelength (excitation), followed by the subsequent emission of secondary fluorescence photons at a longer wavelength. The excitation and emission wavelengths are often separated from each other by a few tens of nanometers [12].

Fluorescence resonance energy transfer is a process by which transfer of energy occurs from an excited state fluorophore to a second chromophore in close proximity in a non-radiative fashion through long-range dipole-dipole interactions. In consequence the gap between the emission wavelength applied on the donor fluorophore and the emission wavelength of the acceptor fluorophore can be enhanced [12]. Proper filtering of the fluorescent signal is therefore facilitated. Because the range over which the energy transfer can take place is limited to approximately 10 nanometers (100 angströms), and the efficiency of transfer is extremely sensitive to the separation distance between fluorophores, resonance energy transfer measurements can be a valuable tool for probing molecular interactions or intra-molecular conformational changes [13].

Resonance energy transfer (RET) is not sensitive to the surrounding solvent shell of a fluorophore, and thus, produces molecular information unique to that revealed by solvent-dependent events, such as fluorescence quenching, excited-state reactions, solvent relaxation, or anisotropic measurements [13]. The major

solvent impact on fluorophores involved in resonance energy transfer is the effect on spectral properties of the donor and acceptor. Non-radiative energy transfer occurs over much longer distances than short-range solvent effects, and the dielectric nature of constituents (solvent and host macromolecule) positioned between the involved fluorophores has very little influence on the efficacy of resonance energy transfer, which depends primarily on the distance between the donor and acceptor fluorophore.

The phenomenon of fluorescence resonance energy transfer is not mediated by photon emission, and furthermore, does not even require the acceptor chromophore to be fluorescent. In most applications, however, both donor and acceptor are fluorescent, and the occurrence of energy transfer manifests itself through quenching of donor fluorescence and a reduction of the fluorescence lifetime, accompanied also by an increase in acceptor fluorescence emission [12]. The efficiency of the energy transfer process varies in proportion to the inverse sixth power of the distance separating the donor and acceptor molecules (see below).

4.2.3 Principles of Fluorescence Resonance Energy Transfer

The process of RET can take place when a donor fluorophore in an electronically excited state non-radiantly transfers its excitation energy to a nearby chromophore, the acceptor. In principle, if the fluorescence emission spectrum of the donor molecule overlaps the absorption spectrum of the acceptor molecule, and the two are within a minimal spatial radius, the donor can directly transfer its excitation energy to the acceptor. A theory proposed by Theodor Förster in the late 1940s initially described the molecular interactions involved in resonance energy transfer, and Förster also developed a formal equation defining the relationship between the transfer rate, inter-chromophore distance, and spectral properties of the involved chromophores [11].

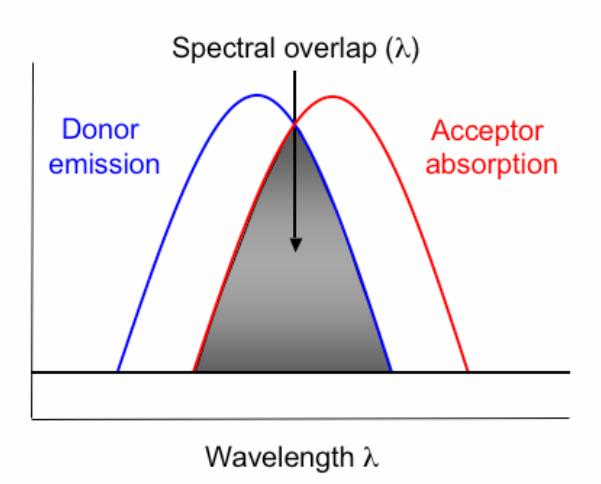

Figure 2: Spectral overlap of donor emission and acceptor absorption (grey)

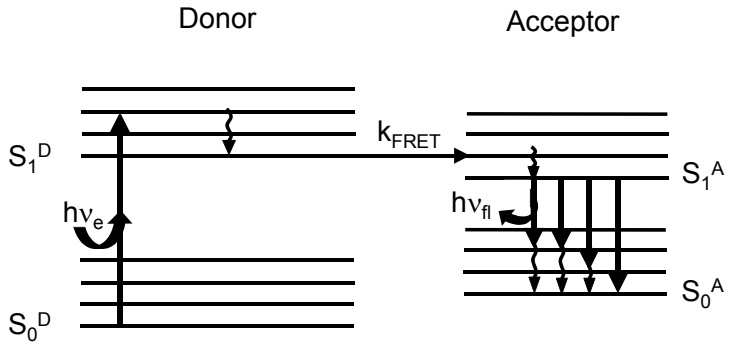

Figure 3: shows a Jablonski diagram for FRET. Fluorescence energy transfer involves two molecules: a donor D and an acceptor A, whose absorption spectrum overlaps the emission spectrum of the donor (see Figure 2). Excitation of the acceptor to the lowest singlet excited state (S_1^D) is a process identical to that described for single-molecule fluorescence. Energy transfer to the acceptor by dipole-dipole interaction, in the presence (within a few nm) of a nearby acceptor molecule, quenches donor fluorescence emission. $h\nu_e$: (donor specific) excitation light; $h\nu_{fl}$: fluorescence emission (acceptor specific); S_0^D: donor singlet ground state; S_0^A: acceptor singlet ground state; S_1^A: acceptor singlet excited state; k_{FRET}: rate constant for FRET.

An alternative detection method, growing rapidly in popularity, is to measure the fluorescence lifetime of the donor fluorophore in the presence and absence of the acceptor.

Presented in Figure 3 is a Jablonski diagram illustrating the coupled transitions involved between the donor emission and acceptor absorbance in fluorescence resonance energy transfer. Absorption and emission transitions are represented by straight vertical arrows, while vibrational relaxation is indicated by wavy arrows. In the presence of a suitable acceptor, the donor fluorophore can transfer excited state energy directly to the acceptor without emitting a photon. The resulting sensitized fluorescence emission has characteristics identical to the emission spectrum of the acceptor [19].

Several criteria must be satisfied in order for resonance energy transfer to occur. As described in equations derived by Förster (and discussed below), the energy transfer efficiency between donor and acceptor molecules decreases as the sixth power of the distance separating the two. Consequently, the ability of the donor fluorophore to transfer its excitation energy to the acceptor by non-radiative interaction decreases sharply with increasing distance between the molecules, limiting the FRET phenomenon to a maximum donor-acceptor separation radius of approximately 10 nanometers. At distances less than 1 nanometer, several other modes of energy and/or electron transfer are possible. The distance dependence of the resonance energy transfer process is the primary basis for its utility in investigation of molecular interactions. In living cell studies involving molecules labeled with donor and acceptor fluorophores, resonance energy transfer will occur only between molecules that are close enough to interact biologically with one another [14].

An additional requirement for resonance energy transfer is that the fluorescence lifetime of the donor molecule must be of sufficient duration to permit the event to occur. Both the rate K_τ and the efficiency E_τ of energy transfer are directly related to the lifetime of the donor fluorophore in the presence and absence of the

acceptor. According to Förster's theory the rate of energy transfer is given by the equation:

$$K_\tau = (1/\tau_D) \bullet [R_0/r]^6$$

where R_0 is the Förster critical distance, τ_D is the donor lifetime in the absence of the acceptor, and r is the distance separating the donor and acceptor chromophores. The Förster critical distance R_0 is defined as the acceptor-donor separation radius for which the transfer rate equals the rate of donor decay (de-excitation) in the absence of acceptor. In other words, when the donor and acceptor radius r equals the Förster distance, then the transfer efficiency is 50 percent. At this separation radius, half of the donor excitation energy is transferred to the acceptor via resonance energy transfer, while the other half is dissipated through a combination of all the other available processes, including fluorescence emission of the donor [11].

The efficiency of energy transfer, E_τ, is a measure of the fraction of photons absorbed by the donor that are transferred to the acceptor, and is related to the donor-acceptor separation distance, r, by the equation:

$$r = R_0 \bullet [(1/E_\tau) - 1]1/6$$

and E_τ is evaluated as:

$$E_\tau = 1 - (t_{DA}/t_D)$$

where t_{DA} is the donor lifetime in the presence of the acceptor and t_D is the donor lifetime in the absence of the acceptor. Therefore, by measuring the donor fluorescence lifetime in the presence and absence of an acceptor (which is indicative of the extent of donor quenching due to the acceptor), it is possible to determine the distance separating donor and acceptor molecules. In many

commonly applied techniques, the energy transfer efficiency is determined by steady state measurements of the relative average donor fluorescence intensities in the presence and absence of the acceptor (not by measuring the lifetimes).

In summary, the rate of energy transfer depends upon the extent of spectral overlap between the donor emission and acceptor absorption spectra, the relative orientation of the donor and acceptor transition dipole moments and the distance separating the donor and acceptor molecules. Any event or process that affects the distance between the donor and acceptor will affect the resonance energy transfer rate, consequently allowing the phenomenon to be quantified, provided that artifacts can be controlled or eliminated.

Energy transfer efficiency is most sensitive to distance changes when the donor-acceptor separation length approaches the Förster distance R_0 for the two molecules. Figure 4 illustrates the $1/r^6$ relationship between transfer efficiency and the distance separating the donor and acceptor. The efficiency rapidly increases to 100 percent as the separation distance decreases below R_0, and conversely, decreases to zero when r is greater than R_0. Because of the strong (sixth-power) dependence of transfer efficiency on distance, measurements of the donor-acceptor separation distance are only reliable when the donor and acceptor radius lies within the Förster distance by +/- 50%. When r is approximately 50% of R_0, the resonance energy transfer efficiency is near the maximum and shorter distances cannot be reliably determined. When the donor-acceptor distance exceeds the R_0 value by 50%, the slope of the curve is so shallow that longer separation distances are not resolved.

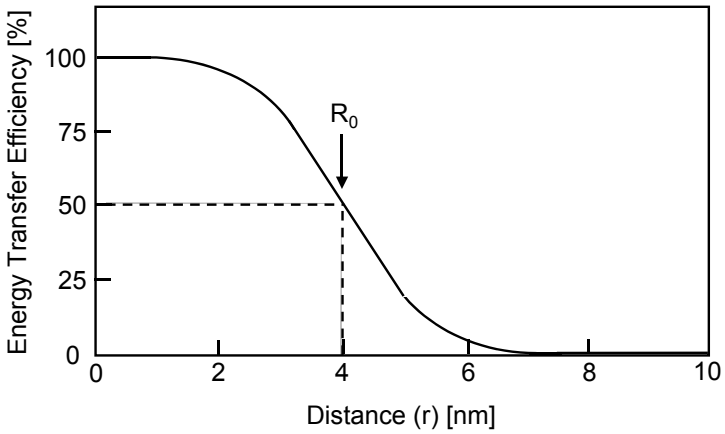

Figure 4: Energy Transfer Efficiency as a function of the distance r (in nm) between the donor and acceptor fluorochrome. At the Förster distance R_0 the transfer efficiency is 50%.

Appropriate donor and acceptor probes are selected on the basis of their absorption and emission spectral characteristics. For maximum resonance energy transfer, the donor emission spectrum should substantially overlap the absorption spectrum of the acceptor. In addition, there should be minimal direct excitation of the acceptor fluorophore at the excitation maximum of the donor, and there should not be significant emission overlap between the donor and acceptor in the wavelength region at which acceptor emission occurs. In practice, it can be difficult to identify donor-acceptor pairs that satisfy these requirements. The situation is often complicated by the fact that the commercially available fluorescence filter sets are not completely effective in passing only the desired wavelengths, and a small percentage of light outside the design passband may be transmitted [15,16,17].

The phenomenon of resonance energy transfer by the Förster mechanism is complex in some aspects, but simple and dependable in its resulting effect.

Förster distances are accurately predictable from spectral properties of the donor and acceptor, and since no exceptions to the theory have yet been identified, resonance energy transfer can be assumed to occur under any conditions that place the donor-acceptor molecule pair in close proximity. The complexity in the theory describing dipole transfer arises, not because of the transfer mechanism itself, but because of the occurrence of distance distributions (including nonrandom distributions), and diffusion of the donor and acceptor molecules [11]. When steps are taken to average the distance dependence of the energy transfer over a range of geometries and timeframes, FRET is a reliable technique for study of the spatial distributions between interacting molecules.

4.2.4 Design of FRET molecules

In order to bypass the background noise of the optical setup that is mostly generated in the optical fiber [ref], fluorescence resonance energy transfer (FRET) is used to achieve a large effective Stokes shift of the fluorescence of the labelled target oligonucleotide sequence which consists of a quintuple thymine base sequence. Thymine was selected because of its low quenching properties compared to the other bases (ref). The 5'-end fluorophore donor was Cy5.5 and the Cy7 fluorophore was used as the 3'-end acceptor. All FRET target molecules where purchased from Genelink, Hawthorne, California, USA Genelink.

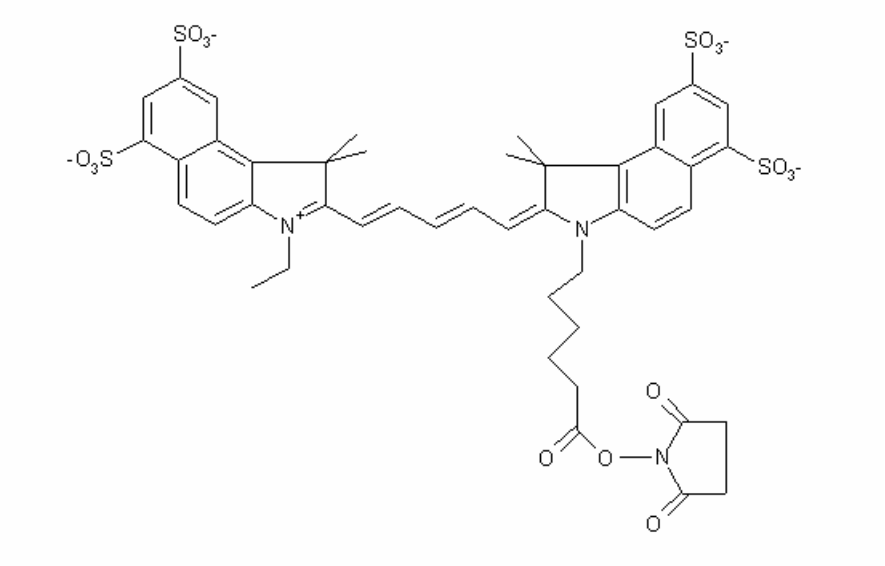

(a)

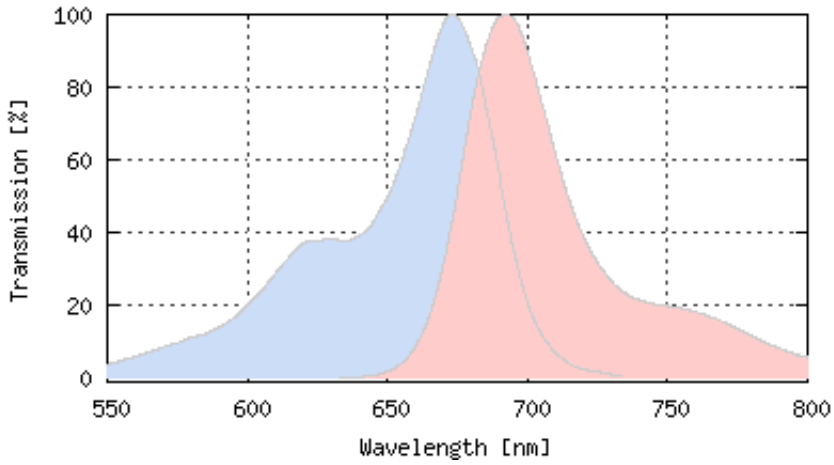

(b)

Figure 5: Molecular structure (a) and absorption/emission spectra (b) of Cy5.5-N-hydroxy-succinimidyl-ester (absorbance max: 675 nm; emission max: 694 nm; extinction coefficient: 250.000 M^{-1} cm^{-1}; Amersham Biosciences 2003)

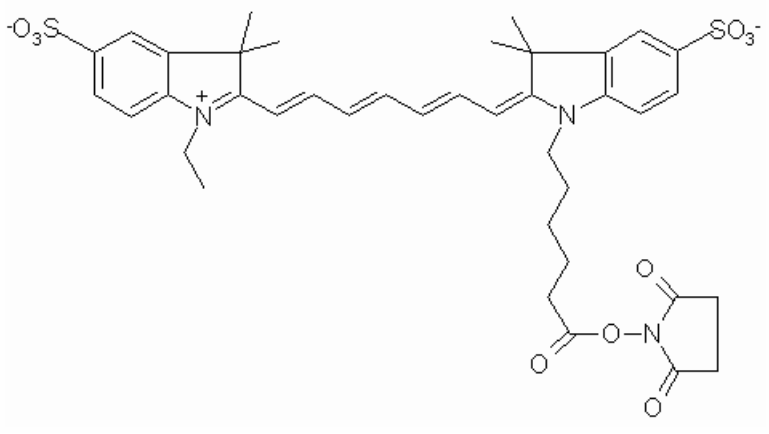

(a)

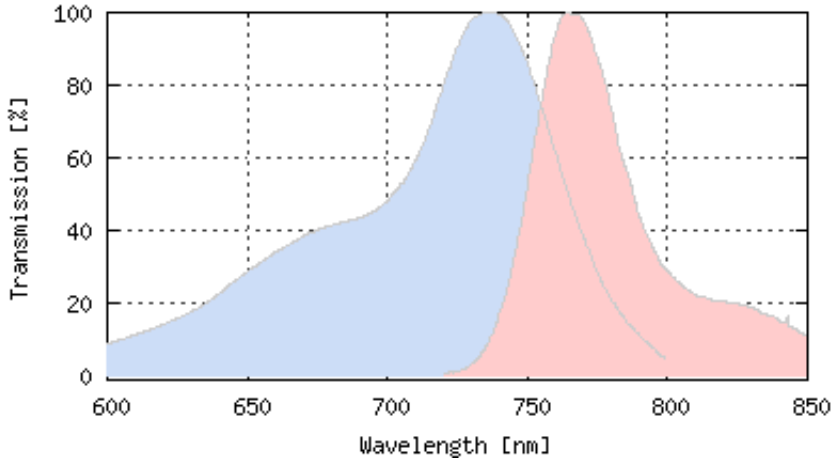

(b)

Figure 6: Molecular structure (a) and absorption/emission spectra (b) of Cy7-N-hydroxy – succinimidyl-ester (absorption max: 743 nm; emission max: 767 nm; extinction coefficient: ~250.000 M^{-1} cm^{-1}; Amersham Biosciences 2003)

4.2.5 Wavelength shifting and filter design

Sending high-power excitation light over an optical fiber bears the disadvantage that inside the fiber background luminescence caused by various effects, like e.g. Raman scattering, is accumulated over the whole length of the fiber [18]. It has

been found that indeed the intensity of the autofluorescence scales linearly with the fiber length.

All spectral measurements were recorded with a USB2000 mobile spectrometer from Ocean Optics Inc. For that matter the SPAD (8) as seen in Figure 1 was replaced by the spectrometer. The cutoff filter (6) was removed and replaced by a holographic notch filter that cuts off the laser line. The excitation power for all fluorophore and background measurements was 2 mW. The integration time for all spectra was 5 sec. A stirring rate of 1000 rpm was chosen to avoid local bleaching. The concentration for both Cy5.5 and oligo FRETs was 50 nM each.

The spectrum of the background shows discrete lines and falls of slowly towards longer wavelengths (see Figure 7). For glass fibers of a length of about 50 cm the amount of background luminescence in the relevant spectral window is so large, that detection of fluorescent molecules, like Cy5.5, excited at 632.8 nm, with a typical Stokes shift of about 50 to 60nm, is impossible since their emission spectrally overlaps with the background spectrum (see Fig. 2). In order to enable the detection of single fluorescent molecules a FRET pair consisting of a short oligonucleotide labelled with Cy5.5 as donor and Cy7 as acceptor is used. The FRET pair can be viewed as an effective chromophore that upon excitation at 632 nm emits fluorescence at 780 nm.

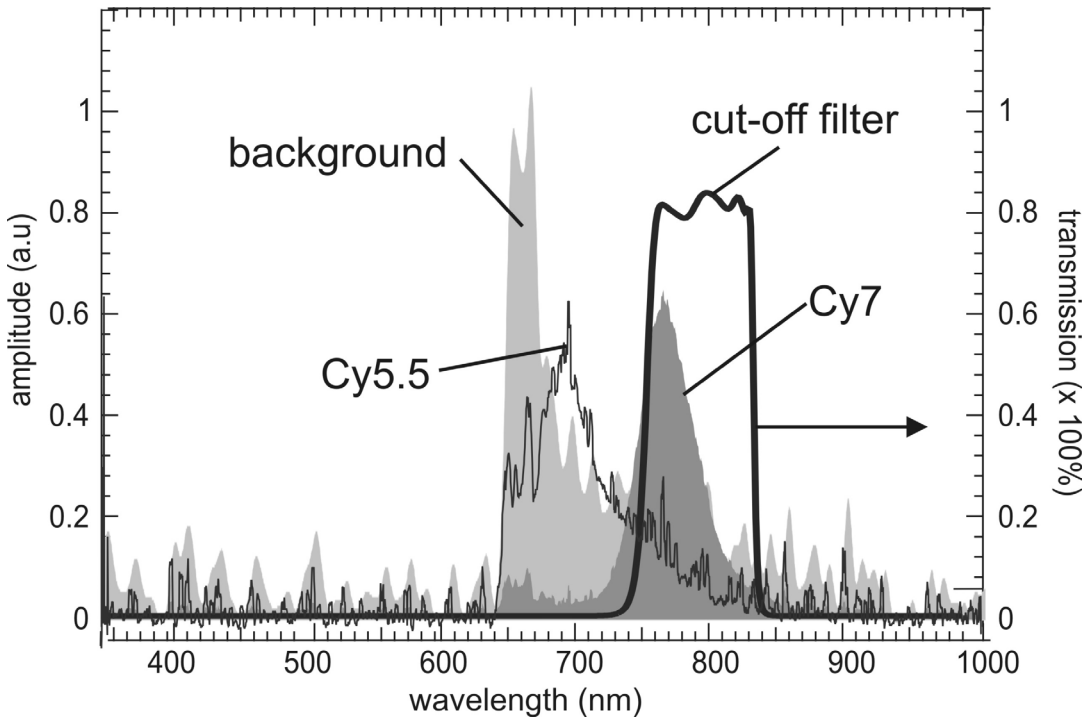

Figure 7: Spectra of fluorophores and filters. Fluorescence spectra have been recorded with the cut-off filter replaced by the notch. Background is the luminescence background of the fiber dipped into a buffer solution. Cy5.5 is the fluorescence spectrum of the dye Cy5.5 plus fiber background. Cy7 is the spectrum of a FRET pair with Cy7 as acceptor and Cy5.5 as donor. Cut-off filter is the transmission characteristics of the cutoff filter used. The wavelength shifted emission of the FRET acceptor Cy7 allows efficient detection while cutting off a significant part of the fiber background.

Using a cut-off filter with a bandpass centered at 795 nm allows detecting a good portion of the fluorescence while cutting off a significant part of the background. As will be shown in the following, this strategy allowed the detection of single FRET pairs through the optical fiber.

4.2.6 Recording of time traces

Data are recorded by counting the number of photons detected for series of subsequent time bins. The bin width was 100μs in all experiments. The total duration of experiments was 1 min if not specified otherwise.

4.2.7 Buffer solution

The oligonucleotides were diluted using a buffer solution containing 10mM Tris-HCl, pH8.3, 50mM KCl, 1.5mM $MgCl_2$ and ultrapure RNAse-free water (Sigma). All experiments were conducted at room temperature.

4.2.8 Data treatment

An algorithm allowing to unambiguously detect transient burst-like signals in presence of stationary noise was programmed in Labview7.1. In order to discriminate a transient signal from the background noise an optimum threshold is determined using an iterative algorithm that isolates the probability distribution of the background noise. Knowledge of the probability distribution of the noise allows excluding the detection of false positive events with a defined probability by choosing a threshold such that for a signal consisting solely of background noise the probability for the detection of a noise peak above the threshold may be neglected. This method was applied to the detection of transient single-molecule fluorescence events in presence of a strong background.

4.2.9 Characteristics of the optical fiber

Figure 8 shows a sketch of the core area of a cleaved optical fiber. The numerical aperture (NA) of the fiber used in the experiments was NA=0.11. This corresponds to a full opening angle of the light cone emitted by the fiber into air of roughly 12°. This angle in turn also is the angle of acceptance for radiation to be coupled into a guided mode. Inside the fiber this corresponds to propagation angle of up to 4.1° that is accepted by the guided mode. The mode field diameter of the fiber is 4.3μm [17].

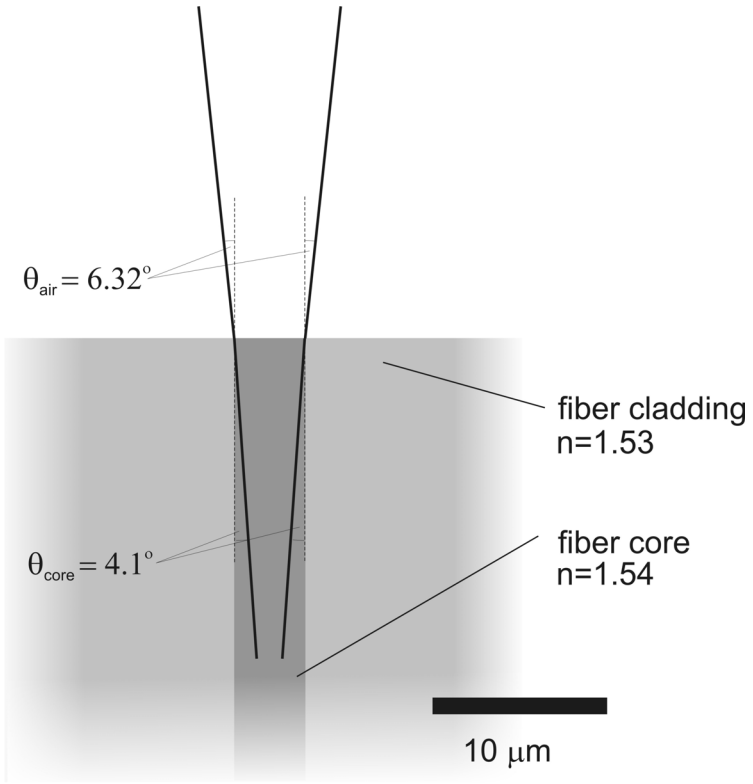

Figure 8: Parameters of the optical fiber.

4.3 Real-time remote detection of fluorescent wavelength-shifting oligonucleotides in liquids through an optical waveguide

4.3.1 Results and Discussion

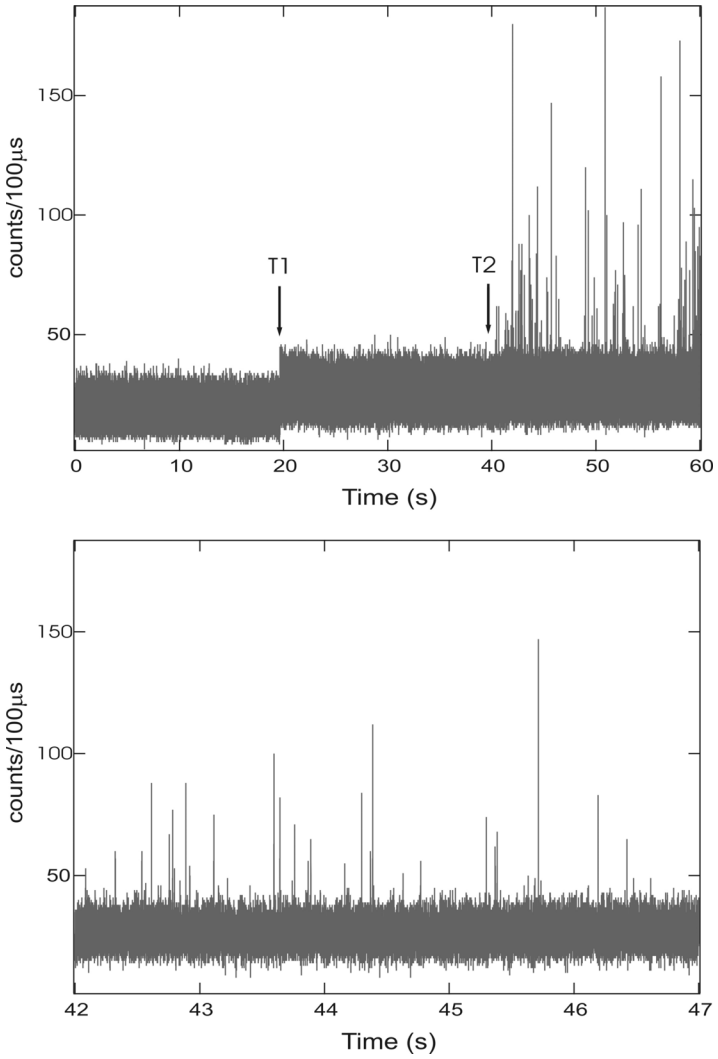

Figure 9: Recording of fluorescence time traces. Upper panel: 60s experiment. The first 20s show signal measured without dipping the fiber into the test solution. At time T1 the fiber dips into the sample solution with a concentration of 1nM. At time T2 stirring (17000 rpm) is switched on and maintained. Lower panel: Zoom into the time trace showing individual fluorescence bursts. Excitation power: 1.8mW.

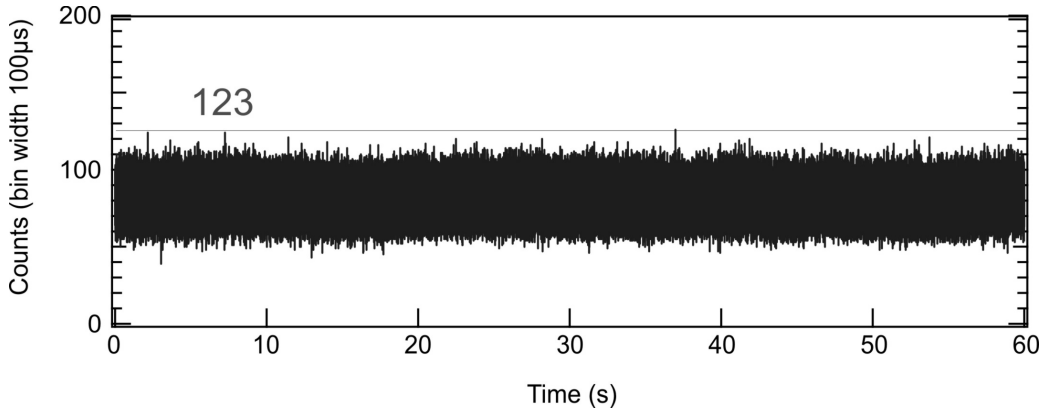

Figure 10: Experiment in a buffer solution with optimal stirring. The line shows the threshold as determined by the burst detection algorithm (chapter 3).

The setup of Figure 1 was used to detect the presence of oligo FRETs in a buffer solution. The fiber was dipped into a test solution containing Cy5.5-Cy7 oligo-FRET molecules in a concentration of 1nM. Figure 9 shows the result of such an experiment. The recording of data was started while the fiber was still in air.

A stable background signal is recorded without any bursts, as expected. At time T1=20s, the fiber is dipped into the test solution. Due to the high concentration of chromophores, the background signal increases slightly. This increase is the cumulative effect of a large number of fluorophores that are excited and couple back their fluorescence into the fiber core. At a concentration of 1nM the average number of FRET pairs in a volume of $1\mu m^3$ is about 0.6. The diffusion constant of a larger molecule in water typically is $D \approx 5 \cdot 10^{-10} \frac{\mathrm{m}^2}{\mathrm{s}}$ (ref) which means that according to $\left\langle x^2 \right\rangle^{1/2} = \sqrt{2Dt}$ a distance of 4µm, which is the diameter of the fiber core, is covered in 16ms. If the diffusion constant is five times smaller, than it already takes 80ms to cover 4µm. This is too long a time for efficient sampling of a larger sample volume [19]. Stirring is used to accelerate this process. At

T2=40s stirring is switched on (17000 rpm). Due to the turbulent flow of the liquid the appearance of fluorescence bursts is observed. The lower panel of Figure 9 is a zoom of a fluorescence time trace showing fluorescence bursts above the background.

Figure 10 for comparison shows the result of an experiment using a clean buffer solution. Although stirring is switched on, no fluorescence events can be detected.

4.3.2 Simulations

The amplitude of the fluorescence bursts observed in Fig. 9 suggests that there is a significant efficiency for the collection of fluorescence by the fiber. To study this light collection process in more detail we consider the radiation patterns of single dipole emitters close to water/glass interface. The refractive index of water is taken to be n_1 = 1.33 – the refractive index of the guiding core is n_2 = 1.54. Once the radiation patterns have been determined, the collection efficiency can be determined by taking the ratio η of the total emitted power by the dipole in the full solid angle and the power emitted into the acceptance solid angle ε for guiding of light in the core. Ω is the solid angle.

$$\eta = \frac{\int_{\varepsilon} p(\Omega) d\Omega}{\int_{full} p(\Omega) d\Omega} \tag{1}$$

Here, $d\Omega = \sin(\theta) d\theta d\phi$ if we assume spherical polar coordinates θ and ϕ. Since θ is counted from the vertical axis, the integrands of (1) have a zero in the direction of the positive and negative z-axis thereby reducing the weight of the radiation in these directions.

Figure 11 shows emission patterns calculated for dipoles far away and in close proximity to the water/glass interface, respectively. Most of the radiation is coupled into large angles close to the angle of total internal reflection (dashed line). Evaluating (1) for these patterns results in $\eta = 0.1\%$ independent of the distance to the interface. This is because the emission pattern in the allowed zone for an infinitely extended interface does not change with distance [18,19]. However, for the case of our fiber, we expect that only molecules with distances sufficiently small compared to the core diameter will significantly couple light back into the fiber.

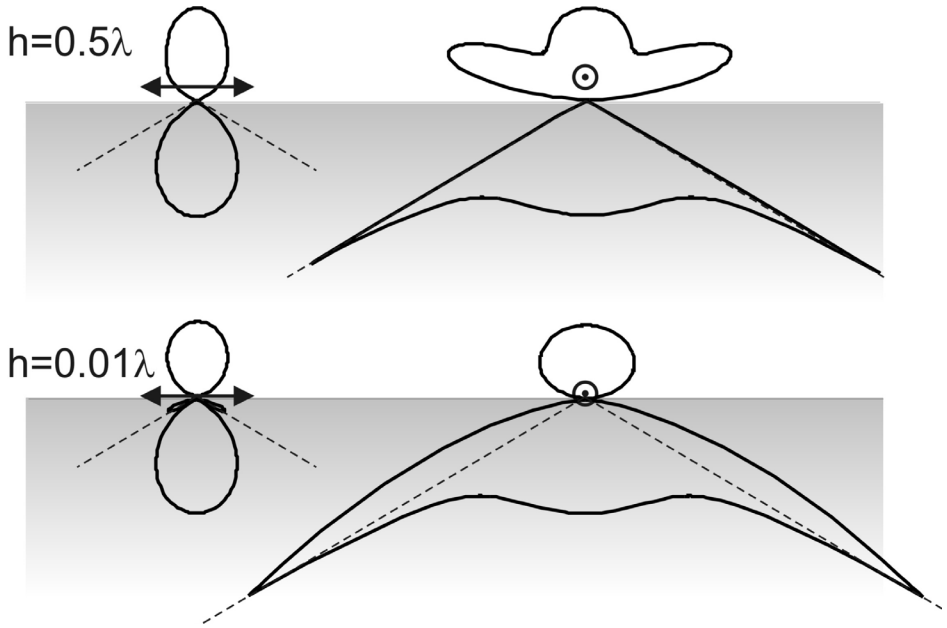

Figure 11: Emission patterns of dye molecules close to an water glass interface, dipole parallel to interface. Upper panel: large distance, lower panel: close proximity. The dashed lines indicate the angle of total internal reflection. Note that the amount of light emitted into the allowed range is independent of the distance to the interface h. Left: cut along the dipole. Right: cut perpendicular to dipole orientation.

The small detection efficiency raises the question how the large fluorescence bursts in Figure 9 can be achieved by considering only a single molecule as a source. The bin width in the time traces of Figure 9 is 100μs and the most probable burst amplitude is between 25 and 50 counts. Taking the collection efficiency of the fiber in account this corresponds to an emission rate of a detected molecule of between $2.5 \cdot 10^8$ and $5 \cdot 10^8$ photons/s. This corresponds to the saturation count rates of two-level systems with excited state lifetimes of between 4ns and 2ns which are compatible with the short excited state lifetimes of Cy dyes of around 1ns. However, this also means that only molecules may be detected which have a negligible triplet yield. In polymers, the triplet lifetimes have been shown to have a large spread, which suggests that a fraction of molecules with small triplet yields might exist [19]. The fast stirring that is necessary to observe significant numbers of peaks would be compatible with such an explanation since the exchange of material is fast enough to allow rare species to be detected at sufficient rates.

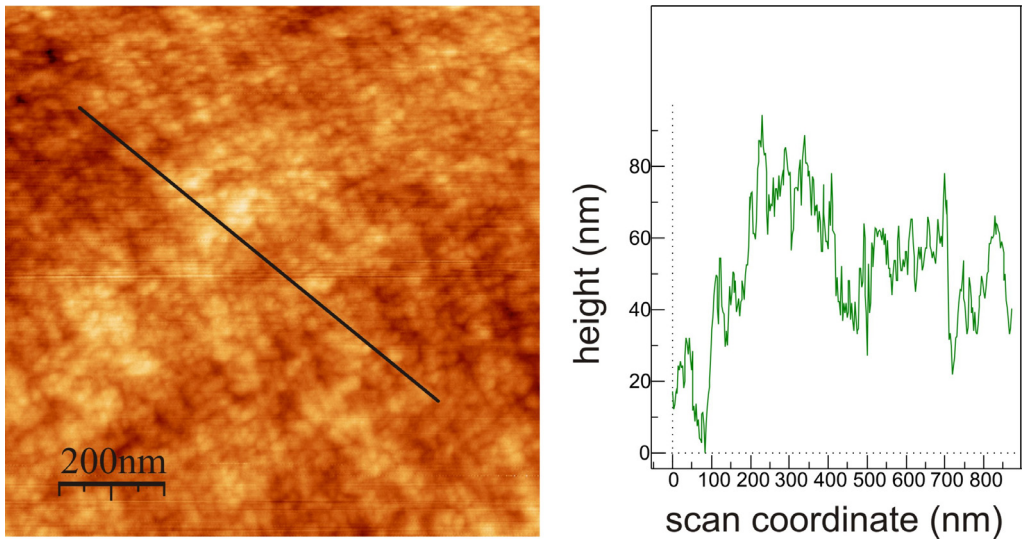

Figure 12: AFM image of the surface of a freshly cleaved fiber end face. Left: topography, right: Line profile along the black line in the topography image. Considerable roughness is observed.

Another explanation for the high amplitude fluorescence bursts might be the fact that the glass/water interface represented by the cleaved fiber is not as smooth as assumed in theory [16,17,18]. Figure 12 shows an atomic force microscopy (AFM) image of an area of a freshly cleaved fiber in the vicinity of the fiber core. Considerable roughness is observed with excursions of up to 20 nm. The effect of such roughness on the emission patterns of single molecules that pass by in close proximity still needs to be investigated in detail using numerical methods.

4.3.3 Conclusions

In this section the possibility to detect single fluorescent oligonucleotide molecules through a glass fiber in a liquid environment has been successfully demonstrated. The continous monitoring of fluorescent signals as a function of time generates characteristic time traces, which show fluorescence bursts that are identified with the signals of single or few fluorophores. The burst detection algorithm can discriminate the bursts from the strong Poissonian background generated mostly in the fiber. The method is capable of performing at room temperature in a conventional lab environment without any special requirements concerning light conditions or sterility. The optical information is gained instantaneously without having to revert to any kind of molecular adsorption procedures. The target molecules are completely free-floating in solution. Up to this point and for next sections to come, the target molecules will remain fluorescent-pre-labelled and for simplicity reasons do not have any switcher function as outlined in the introduction of chapter four. The buffer solution itself is simple to produce and requires no pretreatment whatsoever, nor do the target molecules.

In the next section the influence of various operation parameters and their mutual influences on the performance of the sensor will be discussed.

4.4 Assessment of optimal detection parameters for remote sensing of wavelength-shifting fluorescence-labelled oligonucleotides in liquids through an optical waveguide

4.4.1 Results and Discussion

Influence of the stirring rate

The efficiency of the here proposed method of single-molecule detection and quantification method relies on the ability to acquire a maximum number of events per given duration of the experiment. The goal is to force the maximum number of target molecules to trespass the detection volume of the glass fiber sensor, but still enabling a sufficient number of fluorescence photons to be recorded during a bin width of about 100 µsec. Stirring was applied to a sample solution containing the target molecules (FRET (Cy5.5/Cy7) oligonucleotide ssDNA) to impose a constant flow of liquid across the detection volume. Figure 13 shows different traces recorded at different stirring rates (low at 5000 rpm (a), medium at 12000 rpm (b), high at 16000 rpm (c)), all using the same excitation power (2 mW), bin width (100 µsec) and same concentration of fluorescent target molecules [10 fM]. Two observations can be made comparing the different traces. First of all, the more obvious difference between these traces is the amount of single fluorescent events registered. The higher the stirring rate, the more events occur. This suggests that the higher the stirring rate, the higher the probability for the single target molecules to trespass the detection volume and to produce a fluorescence burst. The second remarkable observation concerns the amplitude of the different bursts. At the optimal stirring rate of 16000 rpm (see Figure 13d) the

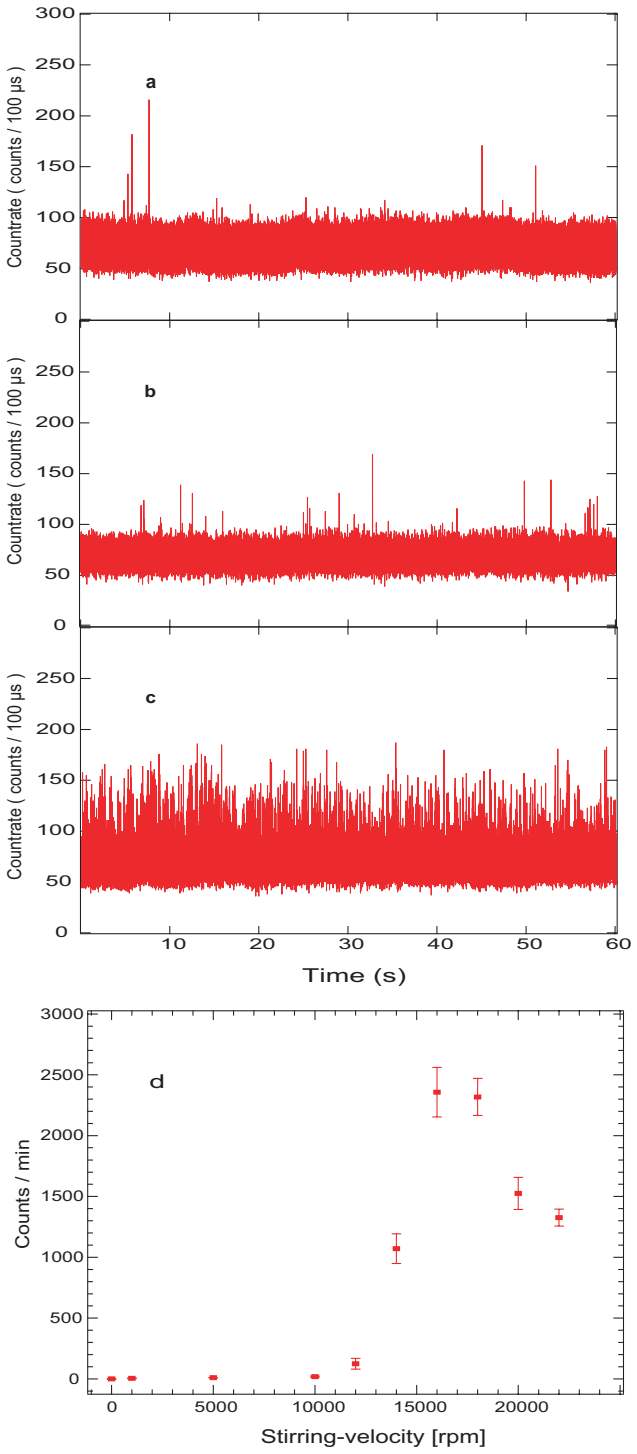

Figure 13: Effect of different stirring rates on the number of fluorescence bursts. (a) was recorded at a stirring rate of 5000 rpm, (b) at 12000 rpm and (c) at 16000 rpm. (d): Number of fluorescence bursts per minute as a function of the stirring rate. Bin width 100 µsec, excitation power 2 mW, concentration of target molecules [10 fM].

amplitude of the majority of the single bursts becomes uniform and almost results in the same amplitude. This amplitude of approximately 50 counts above the background signal sufficiently well correlates with the saturation count rate for single molecules at a bin width of 100 µsec (below, influence of the bin width), presuming the donor fluorophore (Cy5.5) of the FRET pair was saturated at an excitation power of 2 mW and a small fraction of the fluorescence of the acceptor fluorophore (Cy7) is directed into the fiber core [see chapter 4.3]. At a lower stirring rate (b) higher peaks and lower peaks than of a 50 counts amplitude can be observed.

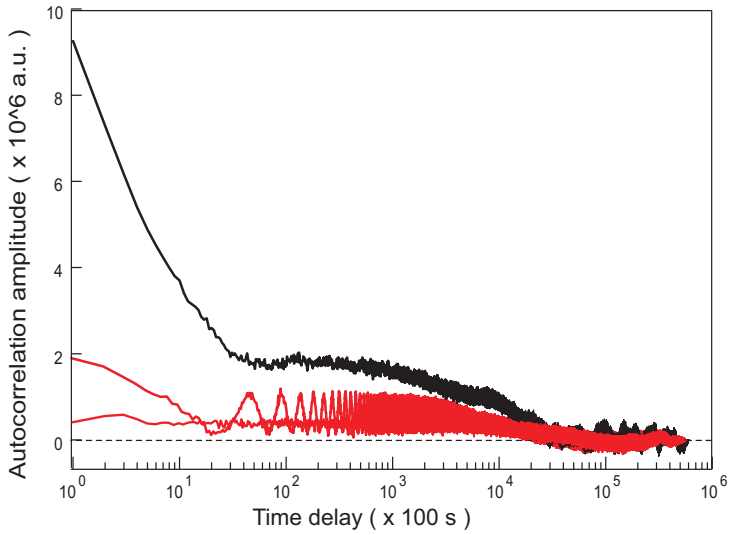

Figure 14: Autocorrelation of the fluorescence time trace as a function of time delay of Fig. 13 (b) (red), 13 (c) (red) and of a time trace which was recorded in plain buffer without target molecules (black). All autocorrelations with an excitation power at 2 mW and a concentration of [10 fM] of target molecules, except for the negative control (2 mW, 16000 rpm, plain buffer solution).

Several target molecules which trespass the detection volume of the sensor simultaneously, provoke a collective signal. Fluorescent bursts of this origin generate much higher amplitude than 50 counts at a bin width of 100 µsec.

Hence, presuming the bin width for both traces being identical, a peak occurring in a time frame recorded at a high stirring rate should appear narrower than one recorded at a lower stirring rate, because of the decreased time available for the molecule to couple its fluorescence back into the fiber. In order to determine the typical duration of a fluorescence burst two time traces at different stirring rates each (12000 rpm and 15000 rpm, respectively) but the same bin width (100 µsec) and concentration of target molecules [10 fM] were subjected to an autocorrelation analysis (Figure 14).
As a negative control an autocorrelation of a time trace recorded with a plain buffer solution, which contained no target molecules, was calculated as well. The autocorrelation shows a mean duration of single bursts of approximately 500 µsec compatible with an optimum bin width of 100µs. The choice of the correct bin width will be discussed in the following section. It has to be mentioned that our detection algorithm does not differentiate between a high or low, expanded or narrow peak. They all will be counted as one burst regardless its amplitude or expansion [see chapter 3]. Collective signals will therefore decrease the total amount of fluorescent bursts recorded during a certain time frame.

In order to properly assess the correct stirring rate for a bin width of 100 µs a series of experiments at a constant excitation power of 2 mW were performed. The glass fiber was dipped in a buffer solution containing fluorescent target molecules at a concentration of 20 fM. The acquisition time for each point was one minute. Five separated measurements were conducted at each stirring rate.

Figure 13 (d). shows the result of the experiment. The optimal stirring rate seems to lie between 16000 rpm and 18000 rpm for the above-mentioned settings. It should be emphasized that poor or no detection of target molecules resulted from using stirring rates below 10000 rpm or no stirring at all, respectively. The intrinsic diffusion is too slow to exchange the whole detection volume in a reasonable amount of time. In addition, it should be considered that a molecule traveling at

such a low speed would probably be bleached instantaneously by the divergent excitation field exiting the fiber tip before it could couple its fluorescence signal into the glass fiber core [13,14]. Using a too high stirring rate (above 20000 rpm) resulted in a decrease of single fluorescence bursts per minute as expected because of a to fast transition of the molecules through the excitation volume.

Influence of the bin width

Data are recorded by counting the number of fluorescence counts that fall in subsequent bins of a certain finite length. Variations of this bin width have a strong influence on the qualitiy and appearance of the data. For too short bin widths, the number of photons per bin decreases which in turn increases the relative importance of shot noise. For too long bins, the time resolution is no longer sufficient to resolve closely spaced peaks. An important aspect of the detection of fluorescence through an optical waveguide is the red-shifted background generated in the waveguide itself [19].

Bin width	Mean background counts per bin	Background noise amplitude	Calculated maximum counts per bin	Signal-to-noise ratio	Detected bursts per min
1000 µsec	3450	59	500	8.5	378
100 µsec	320	18	50	2.8	1281
10 µsec	35	6	5	0.8	726

Table 1: Comparison of bin widths for a fixed stirring rate of 17000 rpm, excitation intensity of 2 mW, and concentration of [5 fM] flurorescent-labelled target oligonucleotide molecules.

The longer the binning time, the higher the mean value of the background and the higher its absolute shot noise amplitude. Since the number of counts that may be extracted per time interval from single molecules is limited, any alteration of the background amplitude will have an impact on the signal-to-noise ratio. To obtain

an estimate for the signal-to-noise ratio we assume the saturation count rate of a single molecule to be approximately $500x10^6$ photons per second [20,21]. Further assuming a detection efficiency of about 0.1% [see chapter 4.3.2] we determine the maximum number of photons recorded in one bin for a single fluorophore to equal 500 counts, 50 counts or 5 counts for binning time rates of 1 msec, 100 µsec or 10 µsec, respectively. Accordingly the signal to noise ratios for the corresponding bin widths can be elicited, considering the amplitude of the background noise of the corresponding bin. The results are documented in Table 1. The signal to noise ratio for a binning of 1 msec would be considered optimal and thus would be expected to result in a maximum of single fluorescent bursts to be detected per time interval. However, experiments conducted with identical settings but variable bin width could not confirm this expectation. At an excitation intensity of 2 mW, a constant stirring rate of 17000 rpm and a concentration of 5 fM fluorescent-labelled target molecules, the highest number of fluorescence bursts was observed for 100 µsec binning. Choosing a too short bin width decreases the signal to noise ratio and therefore result in a loss of the absolute number of counts during a given time frame of one minute because the bursts are prone to fall below the threshold. A too long bin width results in a lower number of detected fluorescence bursts since multiple peaks contribute to only a single burst. This regime should be avoided since the dynamic range of the measurement is being diminished.

The experiments discussed so far were performed at a fixed stirring rate of 16000 rpm and 17000 rpm, respectively. It is expected that the stirring influences the duration of single molecule fluorescence bursts since it influences the velocity at which target molecules pass the detection volume above the glass fiber core. To exclude any influences of the stirring rate on the optimum bin width we have determined the number of fluorescence bursts in a solution containing fluorescent-labeled target molecules at a concentration of 5 fM for different stirring rates. In Figure 15 the number of detected fluorescence bursts during one

minute is plotted as a function of the stirring rate and the bin width. It is clearly visible that among all of the three bin widths investigated, 1 msec nearly consistently shows the lowest number of detected bursts. Surprisingly, for both 100 µsec and 10 µsec bin width a maximum count rate for target molecules during one minute is observed at a stirring rate between 15000 and 20000 rpm. Both bin widths show a decrease of count rates for target molecules at stirring

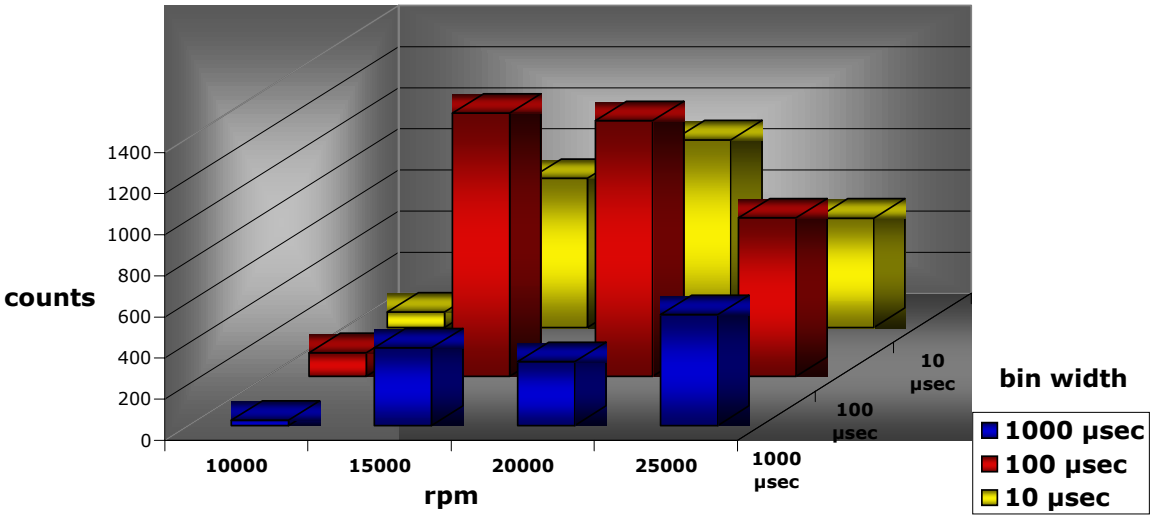

Figure 15: Number of bursts per minute as a function of stirring rate and bin width. Excitation power at 2 mW, concentration of 5 fM target molecules.

rates towards 25000 rpm. It appears that at 25000 rpm or above a majority of molecules pass the detection volume too fast to yield a sufficient signal that could be properly discriminated from the background noise. However for both bin widths a maximum count rate for stirring rates between 15000 and 20000 rpm is observed.

Influence of the Excitation power

Since the emission of photons from individual molecules is subject to a saturation behavior [11,13,19] it is expected that the number of detected fluorescence bursts for a given duration of the experiment will go through a maximum. For low power the burst amplitude will increase linearly with the excitation power. The number of detected bursts above the threshold will slowly increase as well. Once all of the fluorescence bursts are saturated the number of detected peaks can no longer increase. As a matter of fact for further increased excitation power, the background will grow much faster than the fluorescence burst amplitude. Therefore the number of detected peaks will start to deteriorate.

Figure 16 shows traces (a-c) obtained at various excitation intensities at a bin width of 100 µsec, a stirring rate of 17000 rpm and a 10 fM concentration of fluorescent target molecules. The higher the excitation rates in these traces, the higher the mean count rate and the amplitude of the background noise. But remarkably the number of fluorescent bursts increases as well because more and more bursts are detected above the threshold. Figure 16 (d) shows traces obtained at various excitation intensities at a bin width of 100 µsec, a stirring rate of 17000 rpm and a concentration of [10 fM] fluorescent labelled target molecules for any measurement point. The measuring time for every point was one minute. Five separated measurements were conducted at every excitation rate to obtain a mean value. Figure 16 (d) shows that a saturation exists for the needed excitation power beginning at a value of approximately 1.8 mW.

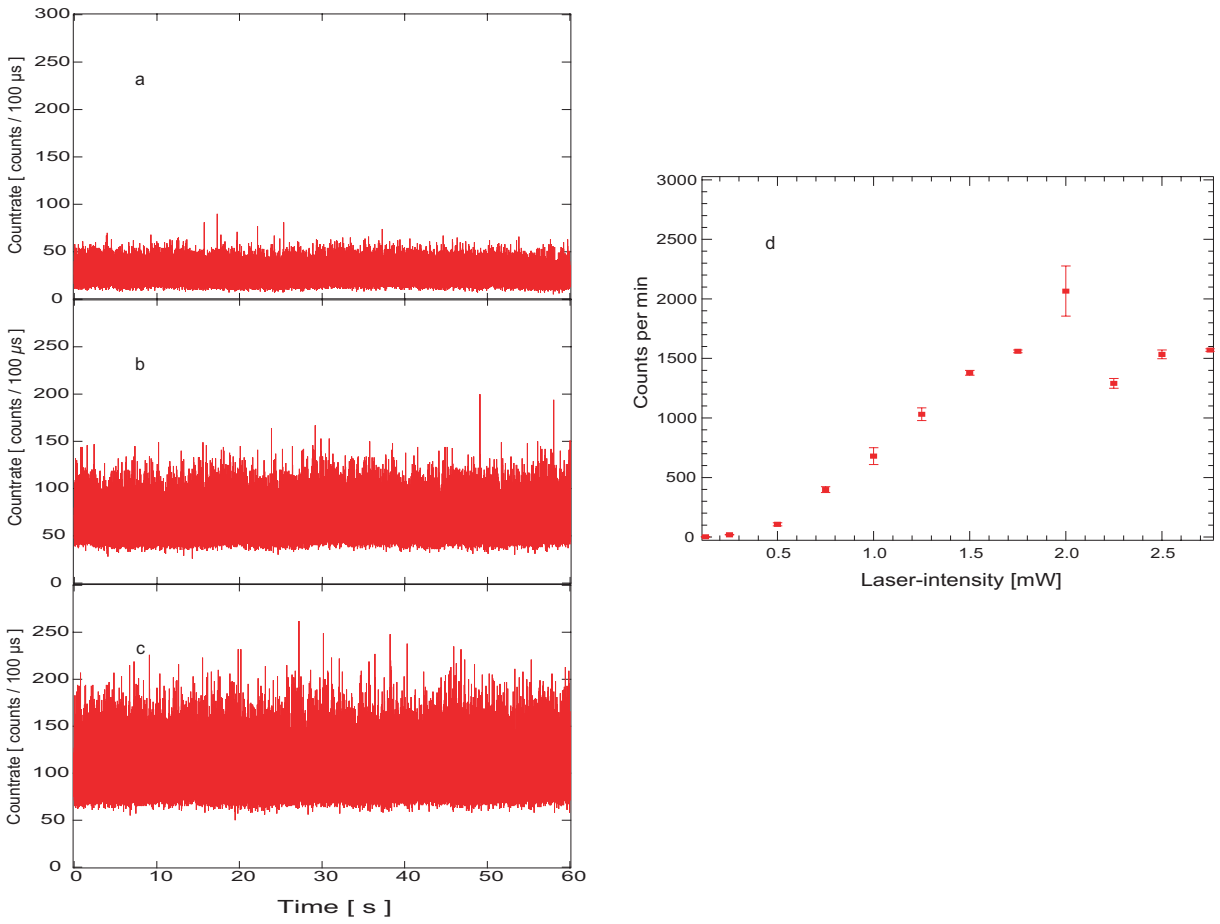

Figure 16 (a-c): Number of fluorescent bursts per minute as a function of time for 500 µW (a), 1.2 mW (b) and 2 mW (c), respectively. Bin width at 100 µsec, stirring rate at 17000 rpm, concentration of target molecules [10 fM]. (d): Number of fluorescent burst per minute as a function of excitation power. Bin width at 100 µsec, stirring rate at 17000 rpm, concentration of target molecules [10 fM]. Note the increasing amplitudes of background and fluorescent bursts with increasing excitation power. For influence on the threshold for proper quantification see chapter 3.

In order to obtain the maximum number of single fluorescent bursts during a fixed time frame it is mandatory to excite the fluorophore FRET pair with a proper excitation power to achieve saturation. For typical fluorophores an intensity of 1 kW/cm^2 is generally considered to be a good estimate for the saturation intensity

for which half of the saturation count rate of a fluorophore is achieved (Figure 17) [11,12,19]. However, to fully saturate a molecule it is necessary to excite at intensities that are up to 10 times larger than the saturation intensity. The diameter of a light guiding glass fiber core at a wavelength of 633 nm measures approximately 4 µm in diameter according to the manufacturer (see chapter 4). For this diameter, 10 kW/cm^2 translate into a power of approximately 1.264 mW. Remarkably, the value needed for the maximum amount of fluorescent bursts per minute as seen in Figure 16 (d) is in the range of 1.8 mW, compatible with the observed saturation in Figure 16.

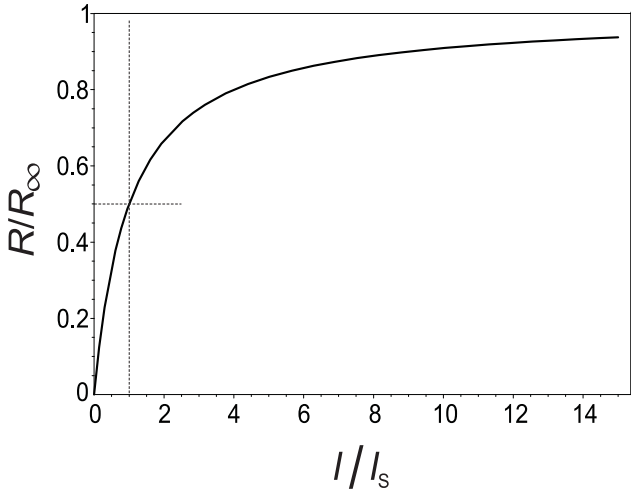

Figure 17: Saturation of the emission rate of a single molecule as a function of the excitation intensity.

Influence of the measuring time

Another crucial parameter is the role of photobleaching in all experiments. Several bleaching experiments were conducted in which different solutions containing the same concentration of fluorescent target molecules at 10 fM were continuously excited at a rate of 2 mW over a period of nearly four hours. The stirring rate for these experiments was at 17000 rpm and a binning time of 100

µsec was used. As shown in Figure 18, the exponential decrease of the fluorescence yield starts almost immediately due to bleaching, yet remains approximately stable during the first five minutes. Therefore the most beneficial moment to record a time trace is immediately after the stirring has been initiated. The maximal time span to acquire single fluorescent signals is 5 minutes.

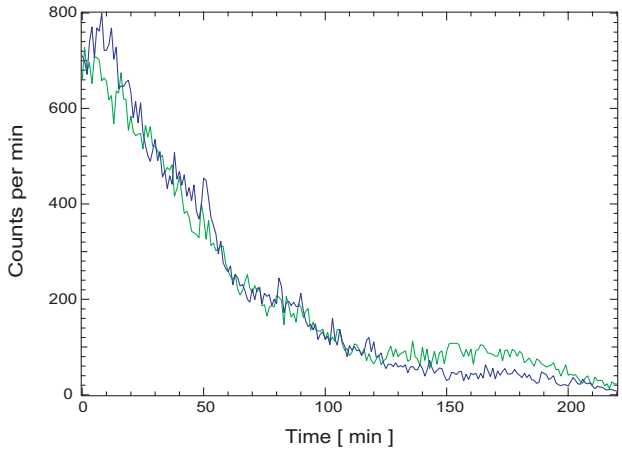

Figure 18: Photobleaching curves of two solutions containing the same concentration of fluorescent labelled target molecules at 10 fM. Stirring rate for these experiments was 17000 rpm and binning time of 100 µsec was used. The photobleaching starts almost immediately yet remains approximately stable during the first five minutes.

4.4.2 Conclusions

Exploring the setting characteristics and their interactions of a new detection system is crucial if a reliable detection method is to be established. The here-performed investigations have demonstrated the importance of the correct choice of settings-parameters for an eventual efficient quantification of targets.

The integration time of 100 µsec to enable the detection of single fluorescence molecule events in liquids was found to be optimal, since the mean duration of a single burst was found to be approximately 500 µsec. A typical fluorescent signal from a single target molecule generates a burst of approximately 50 counts at a bin width of 100 µsec. The stirring rate also plays a crucial role for this detection method. It could be shown that the dependence on the stirring velocity shows a maximum at a range between 16000 rpm and 18000 rpm and that stirring at low rates yields almost no signal at all. Additionally any reciprocal interactions between the bin width and the stirring rate could be excluded. The experiments further showed that the excitation power at the end of the detecting glass fiber needed to be in the order of ten-fold higher than the saturation power of single fluorophores and that it as a matter of fact lies in the range of 2 mW. Additionally it could be shown that the most favorable time span to acquire single fluorescent bursts from a sample solution is during the very first 5 minutes if continuously illuminated.

4.5 Real-time remote quantification of wavelength-shifting fluorescence-labelled oligonucleotides in liquids through an optical waveguide

After extensive investigation of the optical sensor's setting parameters and its potential for single molecule detection of fluorescent target molecules it is now the aim of this section to demonstrate its capabilities for the rapid quantification of target molecules within a timeframe of minutes.
In order to exemplify the dynamic range of the sensor's quantification capabilities and to show a linear dependence of the amount of fluorescent bursts recorded during one minute a dilution series was performed.

4.5.1 Dilution procedure

A dilution step was conducted as follows. In a first step 1/10 (0.1 ml) of the total sample volume (1 ml) was pipetted out of the plexiglass fluid cell and kept in the pipette. The rest of the sample volume was then removed completely from the fluid cell. In a second step the fluid cell was thoroughly rinsed with isopropanol (Sigma) and distilled water for 15 minutes. In a third step the parts of the optical setup that had been in contact with the sample were intensively rinsed with distilled water. In a fourth step the sample that was kept in the pipette (0.1 ml) was reinserted into the fluid cell and 9/10 (0.9 ml) of fresh buffer solution was added.

4.5.2 Results and discussion

In order to adequately being able to distinguish between fluorescent signals due to labeled target molecules and the strong background noise generated by the experimental setup itself [see chapters 4.3 and 4.4], several blank measurements were conducted. Such a measurement is shown in Figure 19(a). The luminescence trace of one minute (inset of Figure 19(a)) acquired in pure buffer in the absence of fluorescent-labeled oligonucleotides shows no single molecule events. The threshold is chosen such that for a given length of the time trace the probability for finding a peak above the threshold is negligible [see chapter 3]. The histogram of Figure 19(a) represents the Gaussian or Poissonian distribution of the background noise [see chapter 3].

At a low concentration [100 aM] of fluorescent-labeled target molecules single bursts can be perceived in the time trace (Figure 19(b, inset)). The bursts clearly pierce through the threshold and can thus be detected and quantified. The histogram of Figure 19(b) visualizes the distribution of the amplitude of the fluorescent signals. The majority of them have a count rate of about 50 counts per bin width (100 µsec), which correlates approximately with the number of fluorescence photons emitted by one fluorophore for near saturation [see chapter 4.4.1], presuming a detection efficiency of 0.1 % [see chapter 4.3.2]. The background signal is also slightly altered. Whereas the mean count rate per bin width (100 µsec) was at 80 counts for the plain buffer solution containing no target molecules (Figure. 19(a)), the mean count rate for the background noise at a concentration of 100 aM is at 110 counts (Figure 19(b)). Additionally the amplitude of the background noise has also increased. Approximately 80 counts for the buffer solution and 95 counts for the concentration of 100 aM. This is due to the fact that the fluorescence of target molecules is contributing to the background noise although they are not passing the detection volume of the

sensor tip themselves. This fluorescence is also registered but does not contribute to fluorescent bursts [see chapters 4.3 and 4.4].

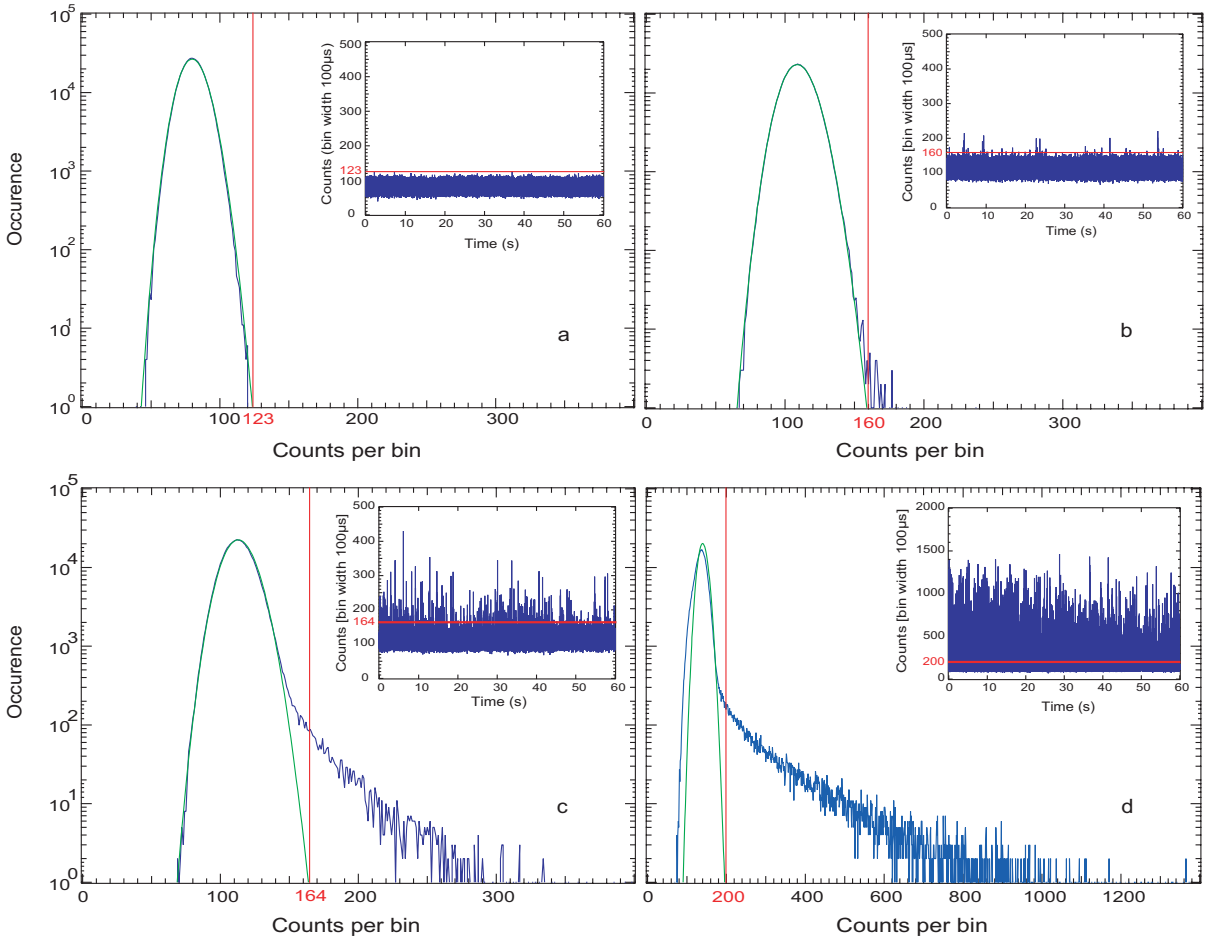

Figure 19: Histograms of the occurrence of fluorescence amplitudes acquired during one minute of measurements. The insets present the time traces recorded for one minute. (a) plain buffer solution containing no fluorescent-labelled target molecules. Concentrations of fluorescent-labelled oligonucleotides: (b) 100 aM, (c) 10 fM, (d) 1 pM. Settings: Excitation power 2 mW, bin width 100 µsec, stirring rate 17000 rpm.

At a medium concentration of 10 fM target molecules (Figure 19(c), inset) the trace changes significantly, compared to the previous one. The most obvious difference is the amount of bursts registered during this one minute, which

already reveals the expected dependence on concentration. In addition, however, the fluorescent bursts also increase in amplitude. This is due to the fact that at higher concentrations the probability of several target molecules to contribute to a collective signal is higher than for lower concentrations [see chapters 4.3 and 4.4]. The fluorescence generated from several target molecules, which trespass the detection volume of the sensor simultaneously, is added up and thus results in a much higher count rate than for single molecules [see chapters 4.3 and 4.4]. The background signal changes compared to the background for the plain buffer measurement for the above-mentioned reasons.

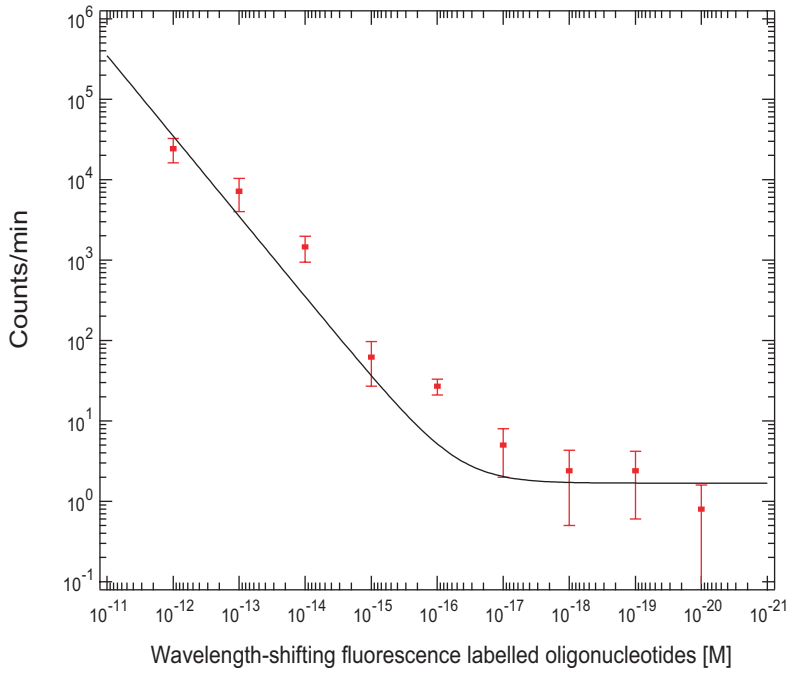

Figure 20: Counts per minute as a function of concentration of fluorescent-labelled target molecules. The measuring time for every point was one minute. Five separated measurements were conducted at every concentration to obtain a mean value. Settings: Excitation power 2 mW, bin width 100 µsec, stirring rate 17000 rpm. Fit function y= ax+b.

Interestingly the fluorescence of this increased concentration (Figure 19(c)) does not contribute significantly to increase the mean count rate or amplitude of the

background trace compared to the background at a concentration of 100 aM (Figure 19(b)). Note only the slight increase of the threshold for the concentration of 100 aM (at 160 counts) compared to the threshold of 10 fM (at 164 counts).

For a high concentration of 1 pM of target molecules however, the trace and the histogram change dramatically (Figure 19(d)), for the above-mentioned reasons.

An extreme increase of the amount, as well as the amplitude of the fluorescent bursts can be observed. Most of the fluorescent bursts consist of collective signals. The mean count rate is now at 140 counts per 100 µsec and the background amplitude even excesses 120 counts per bin. Due to the Poissonian fit of the algorithm the threshold for 1 pM is set at 200 counts.

Comparing all of the histograms with their correlation time traces (Figure 19), high fluorescence bursts appear much more visible in the time traces than in the histograms. This is an artifact of the display. Nevertheless does Figure 19 clearly visualize that through the counting of fluorescent bursts originating from labeled target molecules over a time frame of one minute a quantification of target molecules is possible.

In order to properly assess the range of our detection and quantification method a dilution series was conducted. Figure 20 shows the count rates per bin width (100 µsec) obtained during one minute of recording as a function of the concentration of target molecules. The dilution series was started at a concentration of 1 pM and was conducted for 8 dilution steps, each step diluting the previous concentration by a factor of 10, until a concentration of 10 zM was reached. Already at a concentration of 1 nM the number of fluorescent molecules in volume of $1\mu m^3$ is less then one. For the ultralow concentrations discussed here, stirring of the solution is important to transport molecules into the detection volume.

Every point in Figure 20 represents a number of fluorescence bursts per acquisition interval for a given concentration averaged over 5 acquisition intervals. The acquisition interval for every point was one minute. Figure 20 visualizes the linear concentration dependence of the fluorescent burst count rate gained during one minute of recording. This linear behavior starts at 1 pM and levels off at 1 aM. There is still a detection-sensitivity claimable in the zeptomolar range, a valid quantification however for the sub-attomolar range in 1 minute could not be achieved yet. For longer integration times this should however be possible. For high concentrations in the range of 1 pM, as was shown throughout chapters 4.3 and 4.4, it is quite probable, that several target molecules produce a collective signal, which is counted as a single burst. This decreases the number of potentially measurable counts per time frame and explains the tendency towards higher concentrations to underestimate the true concentration [see chapter 3]. For lower concentrations however, this detection and quantification method proofs to be highly proficient and accurate, since the probability for collective signals is negligible. We emphasize that only one minute is needed to perform a quantification of target molecules. The measurements take place in a liquid environment at room temperature and require no specialized lab equipment. Neither any amplification procedures, such as PCR, nor any pretreatment steps of the sample solution, such as a previous adsorption to a sensor part, are necessary. Additionally the sensor is able to operate with free-floating targets.

4.5.3 Conclusions

The optical sensor is able to detect and quantify single fluorescent-labeled oligonucleotide molecules by discriminating their fluorescence signal from a strong background noise. In order to quantify the amount of labeled molecules contained in a sample solution a trace of counts resulting from single fluorescent bursts as a function of time has to be recorded. The number of bursts recorded during one time trace are then detected by the algorithm introduced in chapter 3 The algorithm does neither take the amplitude nor the time expansion of different bursts into account and thus cannot consider a high or expanded burst as consisting of multiple fluorophores. Although intentionally conservative by doing so the chosen algorithm is suitable for quantification. The performed dilution series shows the linear dependence of the number of fluorescent bursts recorded during a time frame as a function of the concentration. The efficiency of this quantification system ranges from a concentration of 1 pM to 1 aM. It further could be demonstrated that the sensor shows accurate sensitivity for detection of single molecules in the range of zeptomolar concentrations.
The short measuring time that is needed to acquire the data qualifies this procedure as real-time detection and quantification method.

In the next chapter the now established system of optical hardware and algorithm will be combined with molecular beacons. This will insert a molecular switch function into the system. The molecular beacons will operate completely free-floating and be remotely monitored through the glass fiber by the sensor.

4.6 References

1. Milby, K. H. & Zare, R. N., *Am. Clin. Prod. Rev*., 1984, 3, 14-19.
2. Muirhead, K. A. et al., *Biol Technology*, 1985, 3, 337-356.
3. Ansorge, W. et al., *Nucleic Acids Res*., 1988, 16, 2203-2207.
4. Rigler R. et al., J Biotechnolog., 1995, 41, 177-186.
5. Brinkmeier M. et al., Biophys. Chem., 1997, 66, 229-239.
6. Rigler R. et al., J Bioscience, 1990, 3, 180-183.
7. Rigler R. et al., Mets Ue Proc. SPIE, 1992, 1921, 239-248.
8. Lanteri M. *et al.*, *Breast Cancer Res.*, 2005, 7, R487-R494
9. Smith, L. M. et al., *Nature*, 1986, 321, 674-679.
10. Sauer M. et al., J. Chem. Phys. Lett., 1996, 254, 223-228.
11. Zander Ch. et al., Appl. Phys. B, 1996, 63, 517-524.
12. Valeur B. (Ed), Molecular Fluorescence, Principles and Applications, 2002, Wiley-VCH.
13. Feringa B.L. (Ed), Molecular Switches, 2001, Wiley-VCH.
14. Zander Ch., Enderlein J., Keller R.A. (Eds), Single Molecule Detection in Solution, 2002, Wiley-VCH.
15. Gizelli E., Lowe Ch. R (Eds), Biomolecular Sensors, 2002, Tayler & Francis.
16. Jahns J. (Ed), Photonik, Grundlagen, Komponenten und Systeme, 2001, Oldenbourg.
17. Bailey D., Wright E. (Eds), Practical Fiber Optics, 2003, Newnes/Elsevier.
18. Meschede D. (Ed), Optics, Light and Lasers, The Practical Approach to Modern Aspects of Photonics and Laser Physics, 2004, Wiley-VCH.
19. Bachor H.A., Ralph T.C. (Eds), A Guide to Experiments in Quantum Optics, 2004, Wiley-VCH.
20. Novotny L. & Hecht B., *Principles of Nano-Optics, Cambridge University Press*, 2006.
21. Soper S.A. et al., Photochem. Photobiol., 1993, 57, 972-977.
22. Soper S.A. et al., Anal. Chem., 1993, 65, 740-74.

5. Ultrasensitive real-time remote detection and quantification of molecular beacons in liquids via an optical waveguide

5.1 Introduction

In this chapter the previously used fluorescent-labelled oligonucleotides will be completely replaced by molecular beacons (MB). As discussed before, the implication of molecular switches, such as MB [1-2] will assure that fluorescent-labelling of the target molecules and consecutive rinsing of the sample solution will become obsolete. Furthermore a necessary adsorption procedure to a solid interface in order to perform the rinsing will also be rendered superfluous in the first place by the ability of the system to work with free-floating MB [see chapter 4]. The need to absorb the MB to a sensor interface in order to process a fluorescent signal, like with other methods [3-4], can also be disregarded. The high performance of the optical setup to detect concentrations in the attomolar range guarantees that PCR or any other target amplification technique will not be needed [5-7]. In general, a detection system of this kind can be adapted to other relevant biological materials, like proteins, using adequate smart probes based on fluorescence [8]. The combination of single-molecule sensitivity and detection through optical waveguides opens the road for rapid, reliable, ultrasensitive, and cheap medical diagnostics by direct detection of relevant molecular markers [9].
In order for that concept to work a major concern, is the quenching efficiency of the so-called Black Hole Quencher 2 (BHQ2) [see chapter 5.3] used in the following experiments. This is because an incomplete quenching of the FRET donor (Cy5.5) would hinder the sensor to properly discriminate between the on/off-configuration of the molecular switch. Another major challenge is the fact that not all of the MB within the same sample solution are in the closed

conformation at any given moment, even when no targets are present [10]. Although lacking their complementary counterparts a few MB can be in an open conformation for thermodynamic reasons. This is important because the suitable MB/target ratio will have to be determined [see chapter 5.4.3]. Finally, this leads to the last challenge, namely, the ability to perform a quantification of unlabelled, unamplified target molecules by using a fixed concentration of MB. Failure of doing so would mean that previously to a quantification, the needed amount of MB would have to be estimated, which would render the here-introduced method a lot less attractive.

5.2 Molecular Beacons

Molecular beacons (MB) are single-stranded DNA hybridization probes that form a stem-and-loop structure [1-2]. The loop contains a probe sequence (typical length between 20 to 40 bases) that is complementary to a target sequence, and the stem is formed by the hybridization of complementary arm sequences that are located on either side of the probe sequence. A fluorophore is covalently linked to the end of one arm and a quencher is covalently linked to the end of the other arm. Molecular beacons do not fluoresce when they are free in solution. However, when they hybridize to a nucleic acid strand containing a target sequence they undergo a conformational change that enables them to fluoresce brightly (Figure 1).

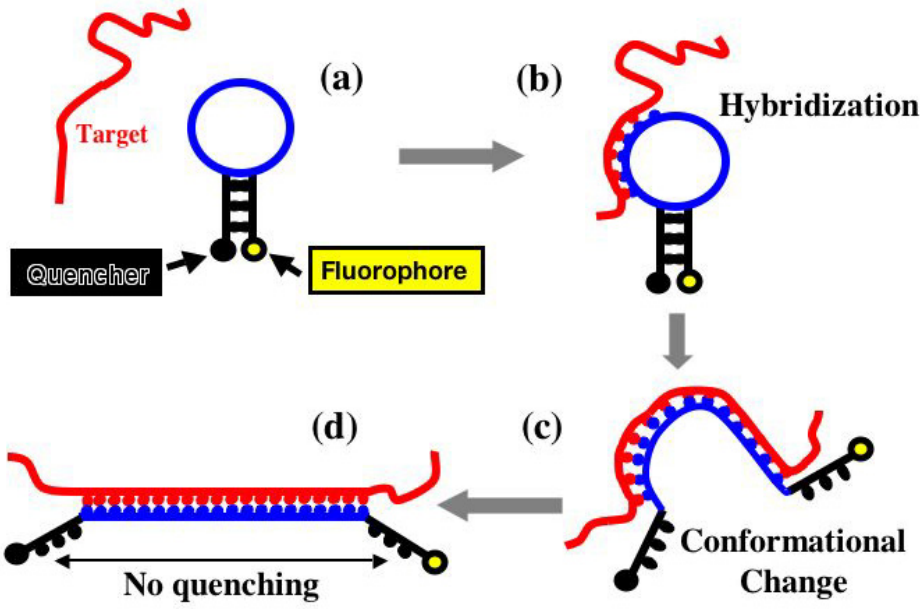

Figure 1: Principle of MB. (a) In the absence of a complementary target the MB remains closed and no fluorescence is emitted. (b-d) When the MB hybridizes to a target molecule, it undergoes a spontaneous conformational change that forces the stem sequences apart and causes the fluorophore and quencher to move away from each other. Since the fluorophore is no longer in close proximity to the quencher, it fluoresces when excited by light.

In the absence of targets, the probe is dark, because the stem places the fluorophore so close to the nonfluorescent quencher that they transiently share electrons, eliminating the ability of the fluorophore to fluoresce [1,2]. When the probe encounters a target molecule, it forms a probe-target hybrid that is longer and more stable than the stem hybrid. The rigidity and length of the probe-target hybrid precludes the simultaneous existence of the stem hybrid. Consequently, the molecular beacon undergoes a spontaneous conformational reorganization that forces the stem hybrid to dissociate and the fluorophore and the quencher to move away from each other, thereby restoring fluorescence (Figure 1(d)).

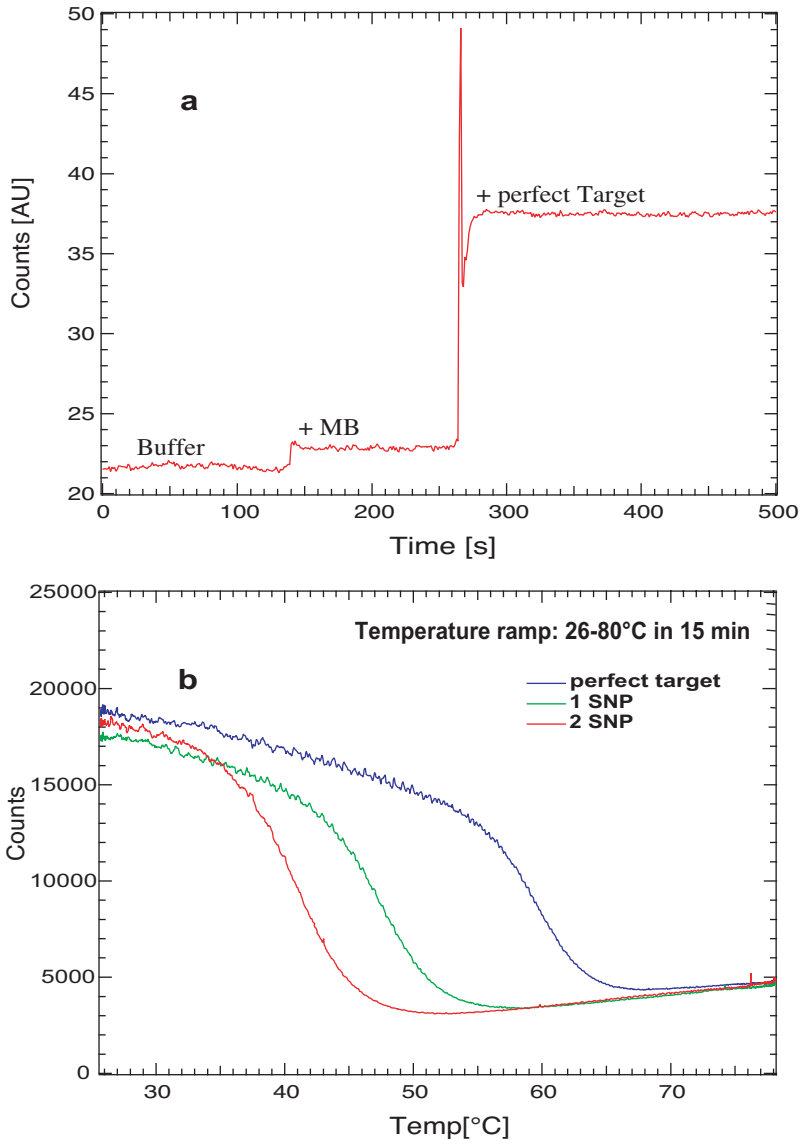

Figure 2: Fluorescence measurement using a Photomultiplier (PMT) and wavelength shifting molecular beacons. (a) Addition of an oligonucleotide complementary to the MB sequence resulted in a massive increase in fluorescence as expected. The peak signal is an experimental artifact resulting from the pipet tip during injection of the target mRNA. (b) Melting curves of MBs hybridized to different target mRNAs with no (blue), one (green) and two (red) single base mismatches (single nucleotide polymorphisms, SNPs). The temperature ramp ran from from 26°C to 80°C in 15 min. This experiment demonstrates the high specificity of the MB.

Using MB even allows for the discrimination of single nucleotide mismatches of target sequences if applied in a temperature controlled environment [10]. Molecular beacons are uniquely suited for the detection of single-nucleotide variations because they recognize their targets with significantly higher specificity than conventional oligonucleotide probes [2,10,11]. Their high specificity is a consequence of their stem-and-loop structure. When a molecular beacon binds to its target sequence, the formation of the probe-target hybrid occurs at the expense of the stem hybrid. Molecular beacons can be designed so that over a temperature range of a few degrees C, only perfectly complementary probe-target hybrids are sufficiently stable to force open the stem hybrid (see Figure 2 (b)). Mismatched probe-target hybrids will not form, except at substantially lower temperatures. Therefore, a relatively wide range of temperatures exist in which perfectly complementary probe-target hybrids elicit a fluorogenic response, while mismatched molecular beacons remain dark. Consequently, assays using molecular beacons robustly discriminate targets that differ from one another by as little as a single nucleotide substitution [2,10,11].

5.3 Experimental

5.3.1 Design of HER-2 mRNA specific Wavelength-shifting MB

Molecular beacons and targets where purchased from Genelink (Hawthorne, California, USA). We took a two-step approach to design suitable wavelength-shifting MB.

For a molecular beacon to be able to find its target sequence in a particular mRNA molecule, the target sequence should not lie within a tight secondary structure or be bound to proteins. Using the RNA secondary structure prediction program MFOLD [12], we identified regions in HER2 mRNA that were either

single stranded or were paired with distant sequences only in most of the thermodynamically favored foldings of HER2 mRNA. We then narrowed the choice of target regions with the help of a second computer program, OLIGOWALK [13], which identifies probe sequences that bind most stably to their complements and cause the least disruption in RNA secondary structure upon binding. The probe sequence with the best binding properties was then selected as the loop sequence for the molecular beacon (Figure 3 (a-d)).

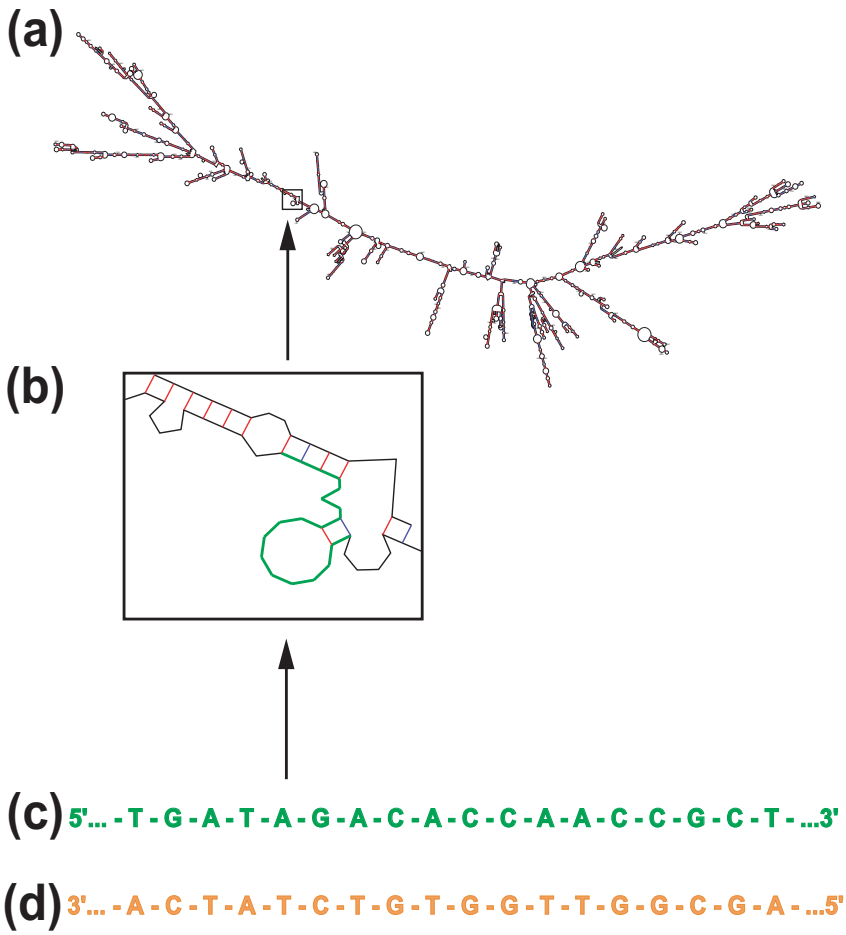

Figure 3: (a) Secondary structure of the linear HER2 mRNA (length: 4530 bases). (b) Region in the HER2 mRNA with favorable properties for MB hybridization (These should be preferentially single stranded, or at least paired with distant sequences only, in most of the thermodynamically favored conformations of HER2 mRNA. (c) Preferred mRNA sequence. (d) Probe sequence, that binds most stably to the preferred mRNA sequence.

In order to bypass autofluorescence excited in the waveguide, wavelength shifting MBs [14] were used. In these structures resonant energy transfer between a donor and acceptor dye is employed to create a huge Stokes shift of the acceptor emission with respect to the donor excitation. The FRET pair consisted of Cy5.5 and Cy7 [15]. BHQ2 was chosen as quencher for the Cy5.5 donor fluorophore [16] (Figure 4 (a)).

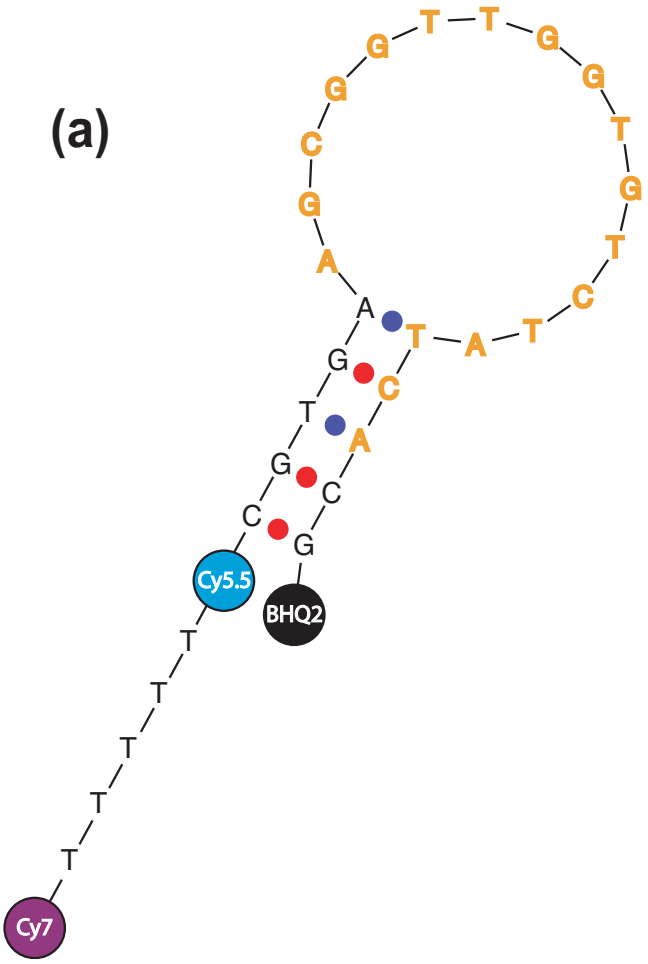

Figure 4 (a): A wavelength-shifting molecular beacon contains three labels: a quencher moiety at the end of its 3' arm sequence (BHQ2), a donor fluorophore at an internal location in its 5' arm that is opposite to the quencher in the hairpin conformation (Cy5.5), and an acceptor (emitter) fluorophore at the distal end of its 5' arm (Cy7).

The donor fluorophore is selected to efficiently absorb energy from the available monochromatic light source. In the absence of targets, these probes are dark, because the energy absorbed by the donor fluorophore is rapidly transferred to the quencher and transformed in heat. In the presence of targets, molecular beacons undergo a conformational reorganization caused by the rigidity of the probe–target duplex, which forcibly separates the 5' arm from the 3' arm. In the target-bound conformation, the energy absorbed by the donor fluorophore is transferred by Fluorescence Resonance Energy Transfer (FRET) to the acceptor fluorophore, which then emits the energy as fluorescent light with a higher wavelength as compared to the wavelength of the excitation light. One limitation of conventional MB was that the optimal emission wavelength was usually only a few nanometers longer than the optimal excitation wavelength. Consequently, a portion of the excitation light could reach the detector by scattering and reflection, thus limiting detection sensitivity. The large shifts of wavelength-shifting MB, allow more effective filtering of the excitation light, thereby enhancing the sensitivity of target detection.

It should be accentuated that the fluorescence signal measured by the photomultiplier (PMT) (J&M, Aachen, Germany), consists of the overall fluorescence yield of all the MB in the open state. In comparison to the fluorescence signal measured by the PMT shown in Figure 2(a), the fluorescence signal acquired with the APD of the optical setup consists of single molecule events. Hereby the photon yield of all open MBs passing by the glass fiber core during one bin correlates to the value of one event. The same experiment that was performed with the PMT (discribed in Fig. 2a) could be reproduced.

5.3.2 Design of synthetic targets

Synthetic targets for the wavelength-shifting MB where purchased at Genelink. The 18 nucleotide long sequence was complementary to the probe sequence of the wavelength-shifting MB. For the melting experiments, targets with one and two SNPs were synthetized.

Sequences:

Perfect target:	TGATAGACACCAACCGCT
Target with 1 SNP:	TGATAGACA**A**CAACCGCT
Target with 2 SNP:	TGATAGACA**AA**AACCGCT

5.3.3 Hybridization Buffer

The buffer used in all experiments contained 10mM Tris-HCl, pH8.3, 50mM KCl, 1.5mM $MgCl_2$ and Ultrapure RNAse-free water (Sigma). All experiments were conducted at 26°C +/- 0^{o}C (regulated by a Labview feedback loop using a thermocoupler, F12 MVCH, Julobo Labortechnik GmbH, Seelbach, Germany).

5.3.4 Optical setup

All experimental hardware and settings were identical to the ones described and determined in chapters 4, if not precised otherwise.

5.4 Results and Discussion

5.4.1 Detection of single wavelength-shifting molecular beacons

As previously shown (see chapters 3 and 4) single molecule fluorescence events resulting from fluorescence-labelled oligonucleotides may be discriminated from a strong normally distributed background. Also, quenching of the FRET signal of the wavelength-shifting molecular beacons is sufficiently strong to allow for a clear discrimination between hybridized and unhybridized MBs. The background signal of the buffer as shown in inset of Figure 2a results only from autofluorescence occurring in the optical setup (mean value of the background signal is 700 counts at a bin width of 100µs). Neither the buffer nor the synthesized targets contribute to an increase of the background signal, as expected. Addition of wavelength-shifting molecular beacons to the buffer solution in the absence of complementary targets results in a slight increase of the overall background (<1%, mean value of the background signal:706 counts at a bin width of 100µs), a phenomenon previously observed in experiments with solutions containing fluorophore concentrations in the pM range and above (see chapter 4). The increase of the background is due on the one hand to imperfect quenching capacity of BHQ2, (quenching efficiency for Cy5.5 is 95% [20]) and on the other hand due to the fact that the probability to find beacons in an open-state at the measurement temperature is not negligible.

The fluorescence F of the solution containing only the molecular beacons can be written as follows [16]:

$$F = \alpha \frac{[B_{closed}]}{B_0} + \beta \frac{[B_{open}]}{B_0} \quad (1)$$

Where $[B_{closed}]$ and $[B_{open}]$ are the concentrations of closed, respectively open beacons with $B_0 = [B_{closed}]+[B_{open}]$ and α and β are the characteristic fluorescence

intensities of the molecular beacons in the closed and open states, respectively. The equilibrium constant K for the opening of the stem loop depends on the temperature T and is given by $K=[B_{open}]/[B_{closed}]$. Using Eq. 1, we have

$$K(T) = \frac{F(T) - \alpha}{\beta - F(T)} \tag{2}$$

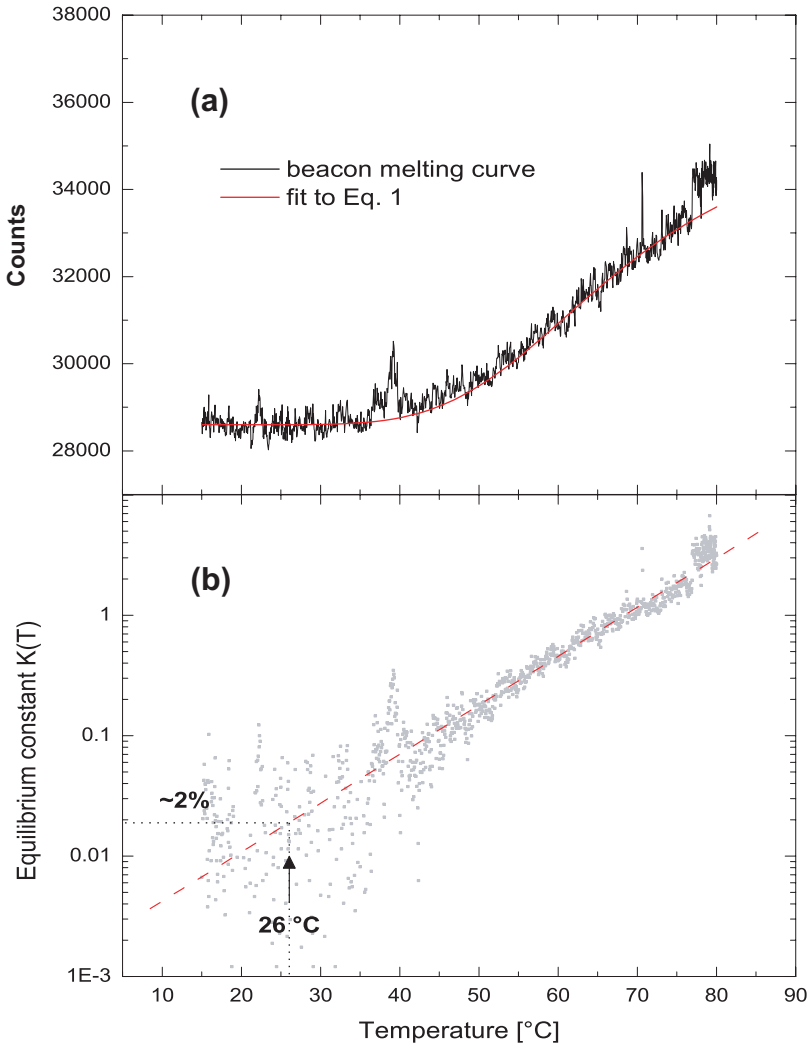

Figure 5: (a) Shows a fit to the melting curve of wavelength-shifting molecular beacons. (b) Shows the equilibrium constant calculated from Eq. 2, using the parameters α and β obtained from the fit.

From the measurements shown in Figure 5b, we can therefore extract the equilibrium constant K(T) giving the ratio of open to closed beacons. The Gibbs free energy change decribing the closed to open state transition of the molecular beacons is given $\Delta G=\Delta H-T\Delta S=-RTlnK(T)$. This approach supposes an all-or-none transition with temperature-independent enthalpy and entropy.

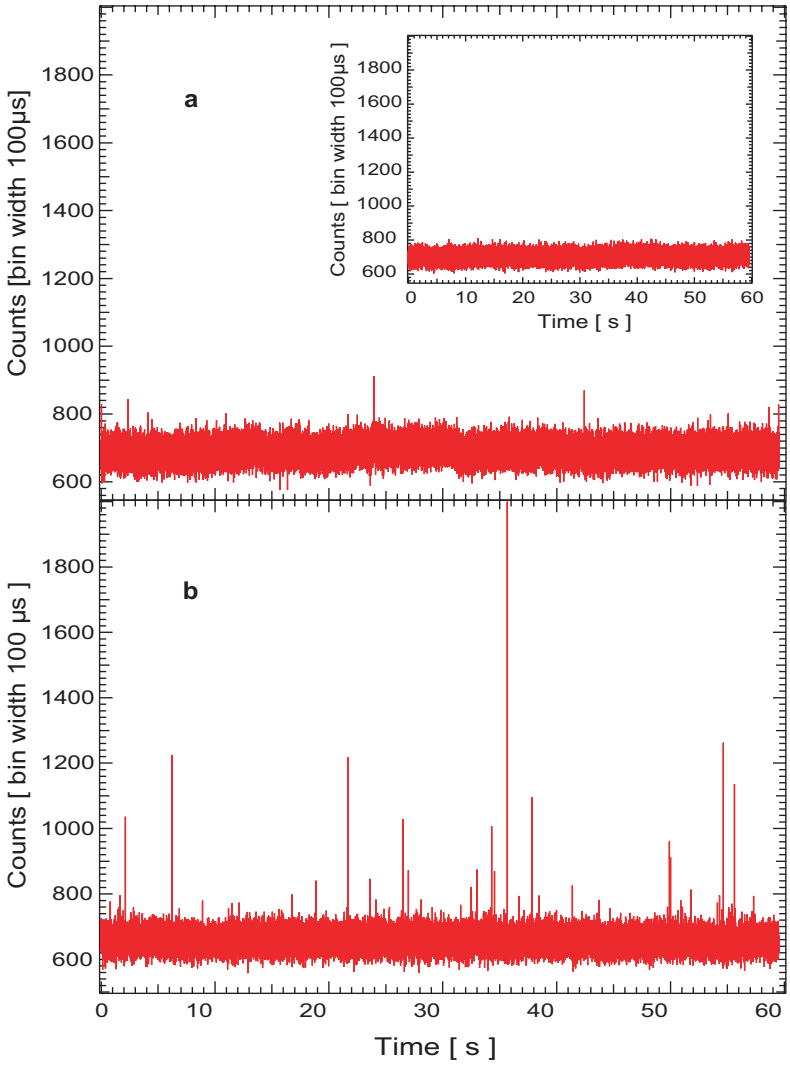

Figure 6: (a) Trace of wavelength-shifting molecular beacons in buffer in the absence of complementary targets. Inset in Figure 6(a): Background fluorescence of pure buffer. (b) Trace of hybridized wavelength-shifting molecular beacons. Settings as described in chapter 4.

A rough estimate of the relevant thermodynamic parameters of the experiment [10] shows that we shall expect about 1-10% of opened beacons at 26°C due to thermal activation. This is in good agreement with the experimental observations. Indeed, the ratio *r* obtained by dividing the number of fluorescence peaks per minute for open beacons in the absence of complementary targets (Fig. 6a) by the number of fluorescence peaks for open beacons hybridized with perfect targets in excess (Fig. 6b) yields $r = 0.09$.

Neither the slight increase of the background nor the small number of bursts observed in absence of targets prohibit the detection and quantification of single-molecule events. Figure 6b shows a trace resulting from hybridization of perfect targets to wavelength-shifting molecular beacons after a hybridization time of ten minutes at a constant temperature of 26°C in a buffer solution. Individual fluorescence bursts produced by the oligonucleotide duplexes are clearly distinguishable from the background signal. The fluorescence bursts vary from 50 till over 1000 counts above the background signal. The amplitude of approximately 50 counts above the background signal correlates optimally with the count rate for one fluorescent burst resulting from one single molecule at a bin width of 100 µsec [see chapter 4]. Peaks having an amplitude of less than 50 counts are highly suggestive for incomplete saturation of the donor fluorophore, inproper fluorescence coupling into the light-guiding fiber core by the acceptor fluorophore or simply because the trespassing of the target molecule through the detection volume of the glass fiber sensor could not be completely acquired during one complete binning interval. The higher peaks occur due to the fact, that sometimes several single molecules trespass the detection volume of the glass fiber sensor during the same binning intervall, resulting in an addition of several small bursts to a bigger one.

It should be emphasized that accurate detection of fluorescent labelled single-molecules in the present detection scheme can only be achieved by proper

permanent stirring of the buffer solution and its components at a high rate [see chapter 4].

5.4.2 Quantification of wavelength-shifting molecular beacons

Figure 7 shows the number of fluorescence bursts as function of the concentration of MB-perfect target duplexes after an initial hybridization time of ten minutes. It results from a dilution series of perfect-targets-wavelength-shifting-molecular-beacons-duplexes in a buffer solution. To assure a quick and proper hybridization of all the wavelength-shifting-molecular-beacons, the ratio of complementary targets to wavelength-shifting-molecular-beacons was 20:1 for the subsequent dilution measurements.

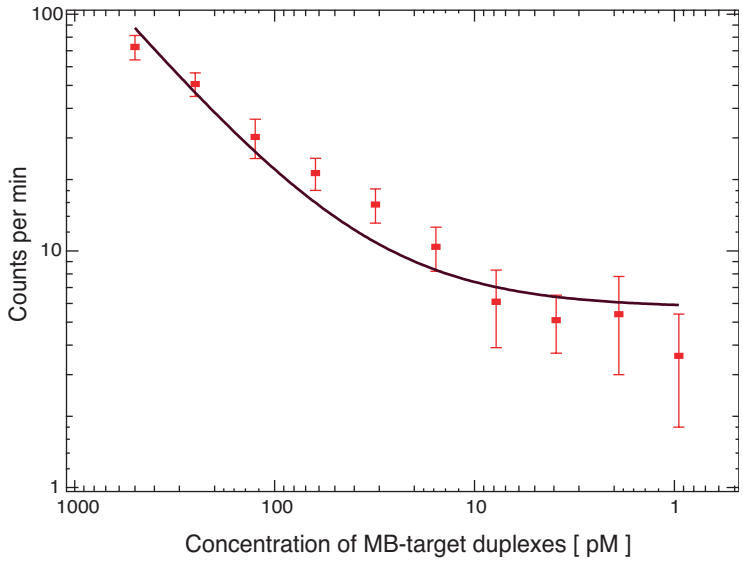

Figure 7: Dependence of the number of fluorescence bursts on the concentration of MB-target duplexes resulting from a dilution series. A concentration dependence of the number of bursts as a function of the concentration is observed between 10 – 500 pM. Below 10 pM the curve starts to level off. Fit function y=ax+b.

Dilution steps were performed by removing for each step half of the sample volume and substituting the missing volume with fresh buffer solution. In order to obtain a mean value, 10 separated measurements of 1 min duration were performed at each concentration. According to previously performed experiments [see chapter 4] we were also able to discriminate single fluorescence bursts resulting from hybridized wavelength-shifting molecular beacons to complementary targets from a strong normally distributed background.

5.4.3 Quantification of complementary targets in relation to a fixed concentration of wavelength-shifting molecular beacons

In order to demonstrate the possibility to quantify the concentration of targets a series of experiments have been performed in which the target concentrations has been increased continuously while the concentration of MBs was fixed at 100pM (see Figure 8). While for small target concentrations the number of detected fluorescence bursts increases linearly with the target concentration at higher target concentrations the number of bursts saturates. This is due to the fact that the maximum number of bursts is limited by the finite concentration of the wavelength-shifting MBs. As expected, concentration of perfect targets higher than the concentration of MB does not result in a further increase of the number of fluorescence bursts detected per minute.

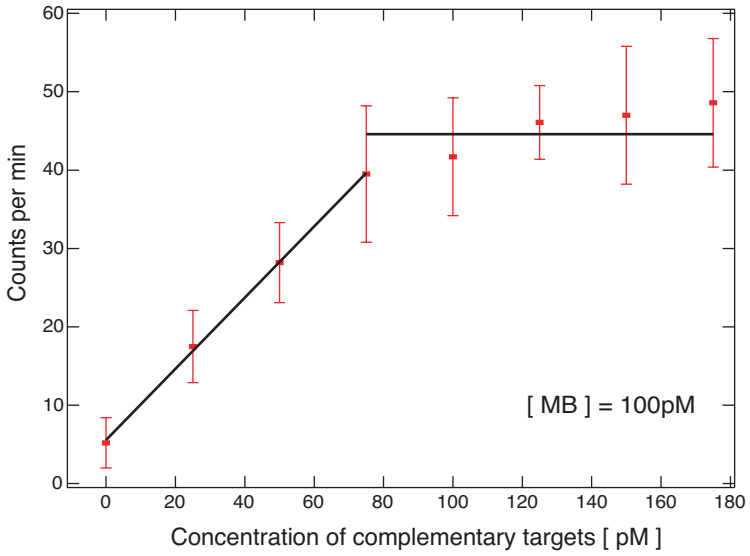

Figure 8: A measurement series with increasing complementary target concentrations (0 - 180 pM) and fixed MB concentrations (100 pM) shows a plateau, since the maximum photon yield is determined by the amount of hybridized molecular beacons and is limited by the fixed concentration of MBs

5.5 Conclusions

In this chapter the MB were successfully integrated into the system. It could be shown that MB lacking their perfect targets do not produce significant additional signals that would interfere with the single molecule detection method. In fact, a solution containing MB in a concentration of up to 100 pM and no targets can hardly be distinguished from a plain buffer solution. The experiments conducted proof that also with MB a linear dependency can be obtained when performing a dilution series. The linear dependency confirms that the sensor is able to quantify free-floating MB-perfect-target-duplexes. In addition, it is also possible to quantify in only one minute the amount of molecular beacons that have hybridized to their target sequence. Furthermore this detection and quantification method can be conducted with a fixed concentration of molecular beacons, which simplifies the procedure, since the amount of MB needed does not have to be anticipated prior to an analysis.

5.6 References

1. Tyagi S. & Kramer R., *Nat. Biotechnol.*, 1996, 14, 303–308.
2. Tyagi S. & Kramer R., *Nat. Biotechnol.*, 1998, 16, 49-53.
3. Fan J. et al., *Chinese Science Bulletin*, 2003, 48, 18, 1903-1905.
4. Fan J. et al., *BioTechniques*, 2005, 39, 583-588.
5. Abravaya K. et al., *Clin. Chem. Lab. Med.*, 2003, 41, 468-474.
6. Antony T. et al. *J. Biomol. Struct. Dyn.*, 2001, 19, 497-504.
7. Broude N.E. et al., *Trends Biotechnol.*, 2002, 20, 249-256.
8. Feringa B.L. (Ed), Molecular Switches, 2001, *Wiley-VCH*.
9. Martha Liley, Optical Transducers (chapter 6), Biomolecular Sensors (Gizeli E. and Lowe C.R., Eds), 2002, *Taylor and Francis*.
10. Bonnet G. *et al*., *Proc. Natl. Acad. Sci. USA*, 1999, 96, 6171-6176.
11. Marras S. et. al., *Genet. Anal*., 1999, 14, 151-156
12. Zuker M. et al., *J. Mol. Biol*., 1999, 288, 911-940
13. Turner D.H. *et al.*, *RNA,* 1999*,* 5,1458-1469.
14. Tyagi S. et al., *Nat. Biotechnol*, 2000, 18, 1191-1196.
15. Marras S. et al., *Nucl. Acid Res.*, 2002, Vol. 30, No. 21.
16. Marras S. et al., *Genet. Anal*., 1999, 14, 151-156.

6. Corollary

The here presented novel detection and quantification method highly qualifies for applications within the biomedical sectors. During the previous chapters the hard- and software has been systematically introduced and tested under various aspects. The algorithm presented in chapter 3 allows for proper discrimination of fluorescent bursts from a strong Poissonian background. Applying this detection method with the correct settings allows for adequate quantification of fluorescent-labelled molecules in solutions. The introduction of molecular switches into the system poses no problems whatsoever, since the quenching efficiency of the BHQ2 is sufficient enough to allow the optical sensor to properly discriminate between the open and closed conformation of the molecular switches. The efficiency of this quantification system ranges from a concentration of 1 pM to 1 aM, which easily surpasses any other oligonucleotide quantification method to date, especially when considering that no amplification such as PCR is needed. It further could be demonstrated that the sensor shows accurate sensitivity for detection of single molecules in the range of zeptomolar concentrations. As intended, chemical immobilization or adsorption procedures can be completely avoided. Since all the detection and quantification measurements were performed using an optical glass fiber, this method can be qualified as remote sensing and offers the potential of parallelization by using different fibers and/or laser wavelengths. It would then be possible to investigate several different targets within the same sample at the same time.

The additional parallel acquisition of different markers, such as life cell markers (e.g. ß-actin, etc.) would allow to simultaneously quantify the measured genetic expression level in relation to a cellular reference value, since the cellular content can greatly vary within different tissue types. The use of glass fibers also enables to separate reusable hardware components from the measuring fluid cell as

claimed in chapter two. The use of integrated optics furthermore ensures the contingency for miniaturization, such as for interests in processing of a lab-on-a-chip. The method is fast. Quantification time rates were all within one minute, which is very rapid comparing today's existing tools in the market. Hence the detection system with its resolution capabilities also reserves the alternative of combination with microfluidic networks.

Considering the fact that up to the probe sequence of the molecular switch the whole system with all its components can be retained unchanged regardless the target sequence of interest, this quantification method allows for an even broader spectrum of supplementary applications. Other possible fields of interests additional to the pharmaceutical and biomedical fields would be the farming sector, e.g. varmint detection, materials research, e.g. investigation of repellent surfaces and of course the military sector, e.g. the detection of ultralow concentrations of bioagents.

7. Molecular Beacons and perfect targets in hemolyzed blood: an outlook

7.1 Introduction

Circulating RNA in plasma/serum is an emerging field for noninvasive molecular diagnosis [1-4]. Problems for fluorescence-based detections methods, however, may arise if the absorbance and emission spectra of hemoglobin would crosstalk with a test system of fluorochromes [5-7]. However initial experiments using perfect HER2/Neu mRNA-molecules as targets that have been spiked into a blood citrate-lysate sample indicate that the biosensor might also work in life tissue containing corresponding molecular beacons. The molecular beacons were able to find their targets even in presence of unspecific RNA and DNA within minutes. A presumed interference by autofluorescence of hemoglobin lead to no artifacts whatsoever.

7.2 Experimental, results and discussion

The here presented detection and quantification method has been conceived to operate in a clinical environment. However the step from the bench to the bedside still needs considerable efforts. Nevertheless a preliminary rough check measurement was conducted. The molecular beacons and perfect targets used in chapter 7 were used accordingly to their previously described specifications. The buffer solution was completely replaced by blood. The blood was extracted imminently before the experiment and stored in a citrate-containing syringe. The blood was then subsequently hemolyzed with a drop of conventional liquid soap. The so hemolyzed blood sample was then placed in the fluid cell. After a brief phase of homogenization the fiber sensor was placed into the blood sample and the molecular beacons were added, 14 seconds after the recording had been

started (Fig. 1 (a)). A slight increase of the background mean count rate can be determined, due to imperfect quenching of the FRET pair (see chapter 7). The amplitude of the background however does practically not change. After 60 seconds the recording was restarted in order to maintain the data file down to a manageable size. After 70 seconds of the restarted recording the perfect targets were added (Fig. 1 (b), I). Although for reasons of display barely visible, a slight increase of the background can also be observed.

Then the first hybridized beacons yield their fluorescent signal into the glass fiber. But it is only after almost 3 minutes that the majority of the molecular beacons starts to hybridize to their targets. This causes a massive increase of the background mean count rate and the amplitude as described in chapter 6 for the FRET target molecules. The single fluorescent bursts are clearly distinguishable from the background. In addition, some bursts consisting of collective signals can be perceived, as described in the previous chapters. The main concerns with this experiment were that remains of corpuscular elements within a liquid solution would cause measuring artifacts by colliding with the glass fiber sensor or that the autofluorescence of the hemoglobin molecules might interfere with the FRET signal. Neither was the case.

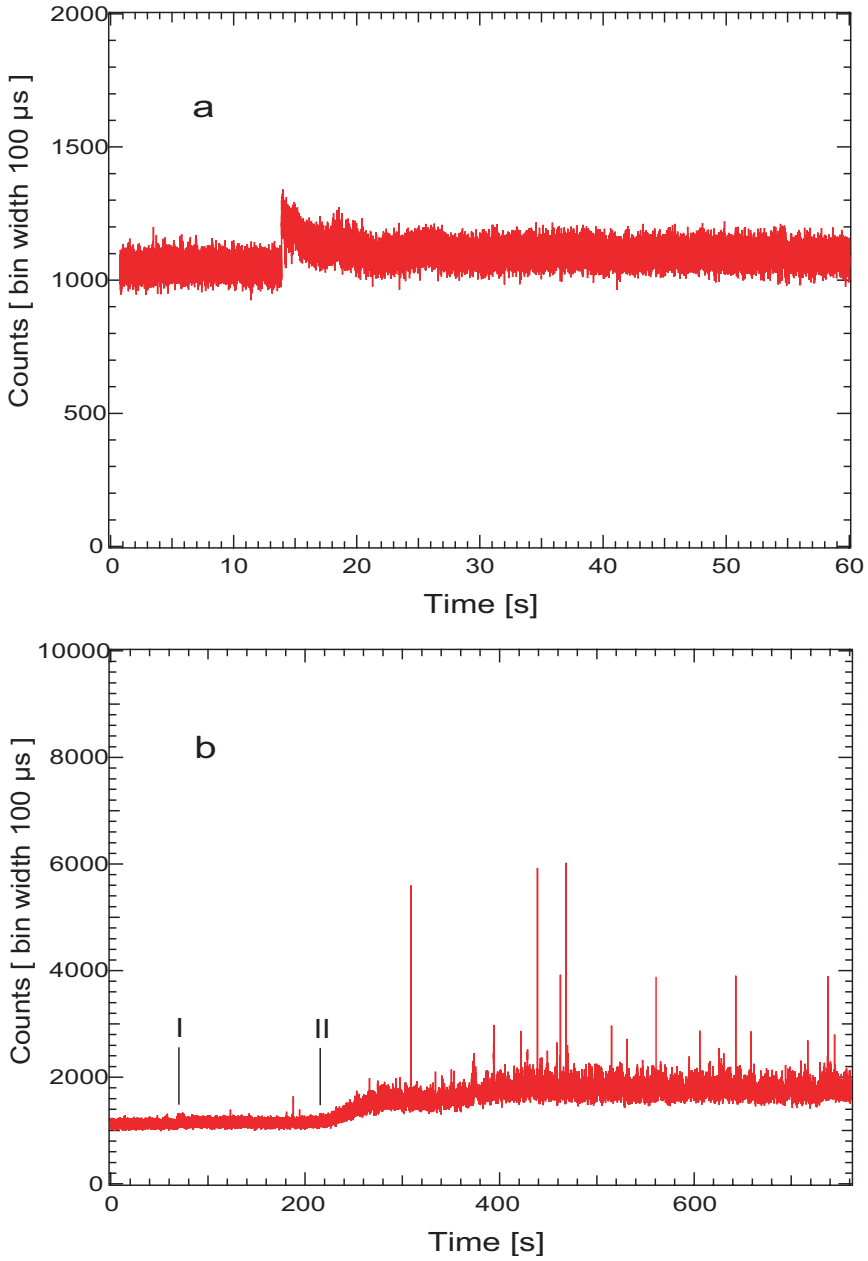

Figure 1(a) and (b): Contiguous acquisition of counts (bin width 100 µsec) as a function of time for a demonstration of a real-time hybridization of molecular beacons to their perfect HER2/Neu target mRNA-molecules in hemolyzed blood. Insertion of molecular beacons (a) after 14 seconds of experiment time. Insertion of perfect mRNA targets after 70 seconds of the restarted experiment recording (b,I). Begin of hybridization (b,II). Settings as described in chapter 4 and 5.

7.3 Conclusions

In summary, our preliminary experiments show, that our approach is capable of highly sensitive, highly accurate detection of perfect HER2 mRNA target molecules within few minutes using molecular beacons in hemolyzed blood. The main concern hereby was that remains of corpuscular elements within a liquid solution and the hemoglobin would cause measuring artifacts. The results however are quite encouraging, since neither the suspected autofluorescence from hemoglobin molecules nor any membrane residuals would provoke any disturbances.

7.4 References

1. Dasi F. et al., *Lab. Inves*., 2001, 81, 5.
2. Enders K. O. et al., *Clin. Chem*., 2002, 48, 8, 1212-1217.
3. Tsui N. et al., *Clin. Chem*., 2002, 48, 10, 1647-1653.
4. Chen XQ. et al., *Clin. Cancer Res*., 2000, 6, 3823-3826.
5. Chance B. et al., *Rev. Sci. Instrum*., 1998, 69, 10, 3457-3481.
6. Zhang J. et al., J. *Photochem. Photobiol*., 1988, 1, 329-335.
7. Sato H. et al., *J. Biomed. Optics*, 2001, 6, 366-370.

8. Technical Drawings

In the following some of the plans produced by the workshop of the technical department of the Institute of Physics are presented. These blueprints show the design of the stirring device of the optical setup. In order to achieve rates of up to 25000 rpm, the demands for this device were very conservative. The stirring had to be performed at an adjustable rate, which was controlled by a specially designed experiment control software. The device mainly consists of a motor and a downstream tachometer. The also specially produced PMMA fluid cell could be fixed flush to the stirring device in order to avoid evaporation of the sample solution but had also to be operational in an open position to allow for proper diluting of solutions while the sample would be stirred constantly. Additionally the glass fiber sensor had to remain in an identical position for all measurements. Sample compartment is able to contain up to 1.5 ml of sample. However, most of the measurements were performed with an amount of 1 ml, if not precised otherwise.

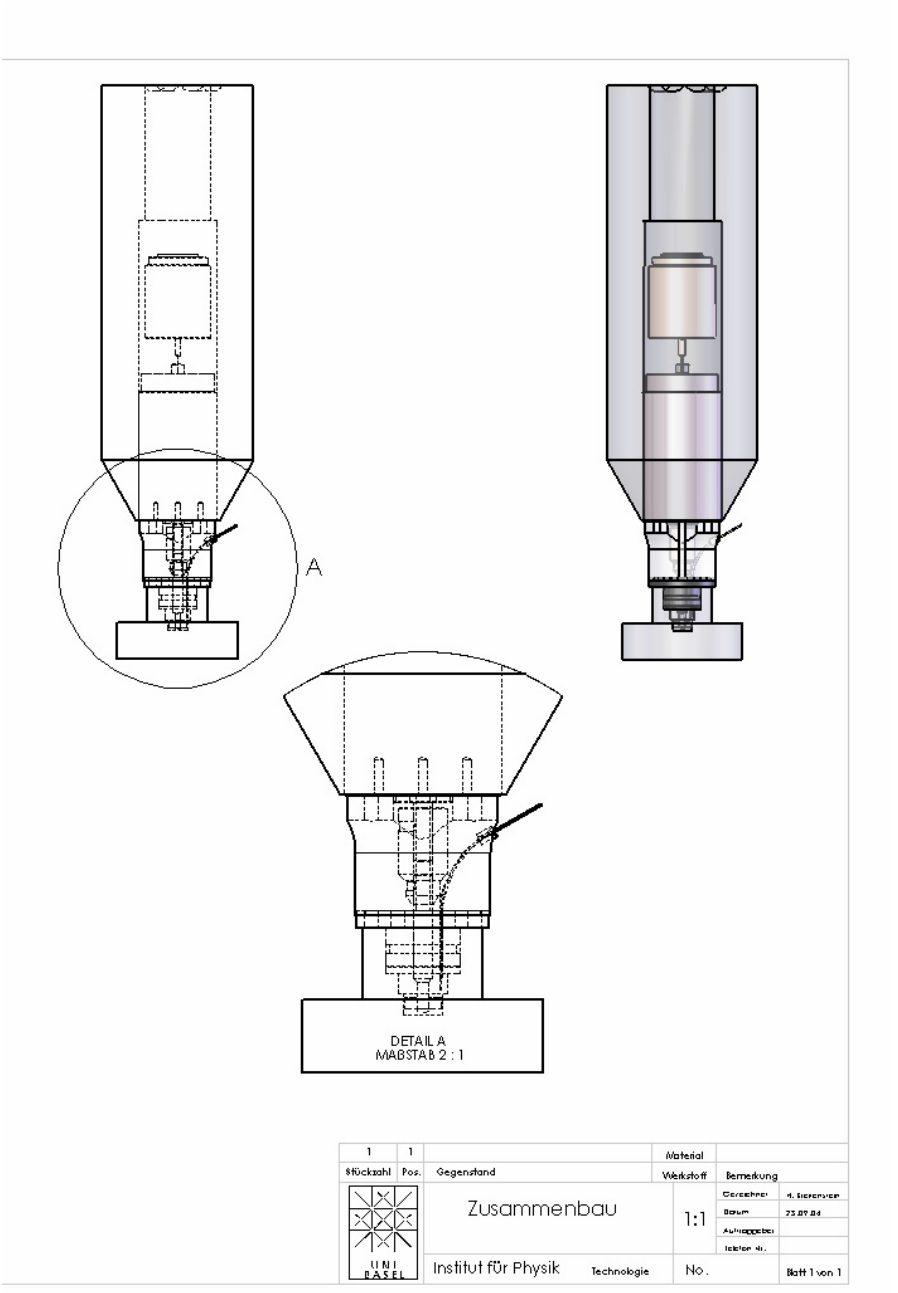

Figure 1: Shows a blueprint of the main compartment of the stirring device with a magnification of the transition in the area of stirring axle. Note the insertion channel for the glass fiber sensor.

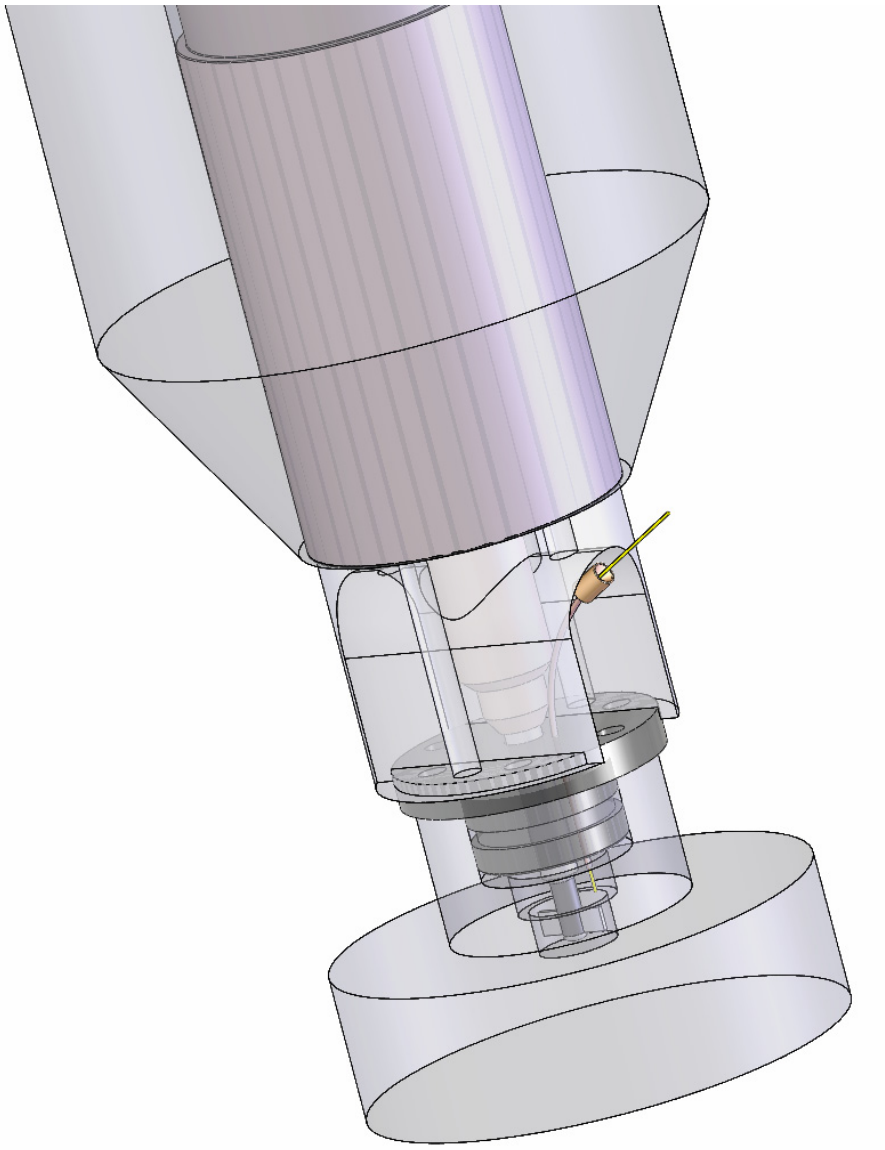

Figure 2: This blueprint demonstrates the configuration for measurements under tight sealing of the plexi glass fluid cell. This setup configuration was chosen when sample evaporation had to be avoided, e.g. for the bleaching experiment (see chapter 4) or at least minimized, since the axle channel to the sample compartment was intentionally not perfectly sealed.

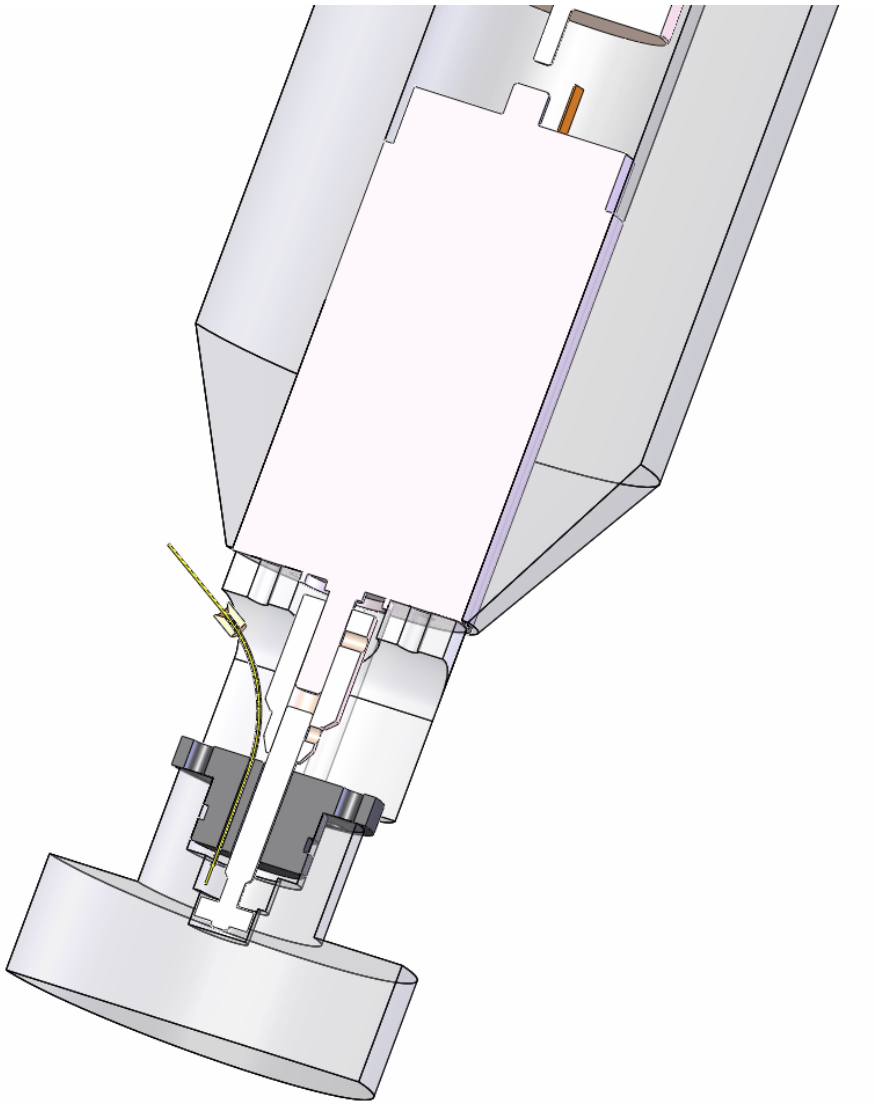

Figure 3: Cross section through the stirring device and plexi glass fluid cell. This Figure visualizes the relative position of the glass fiber sensor to the stirring blade. It also shows the sample compartment below the sealing cap (dark grey). Note the channel of the glass fiber.

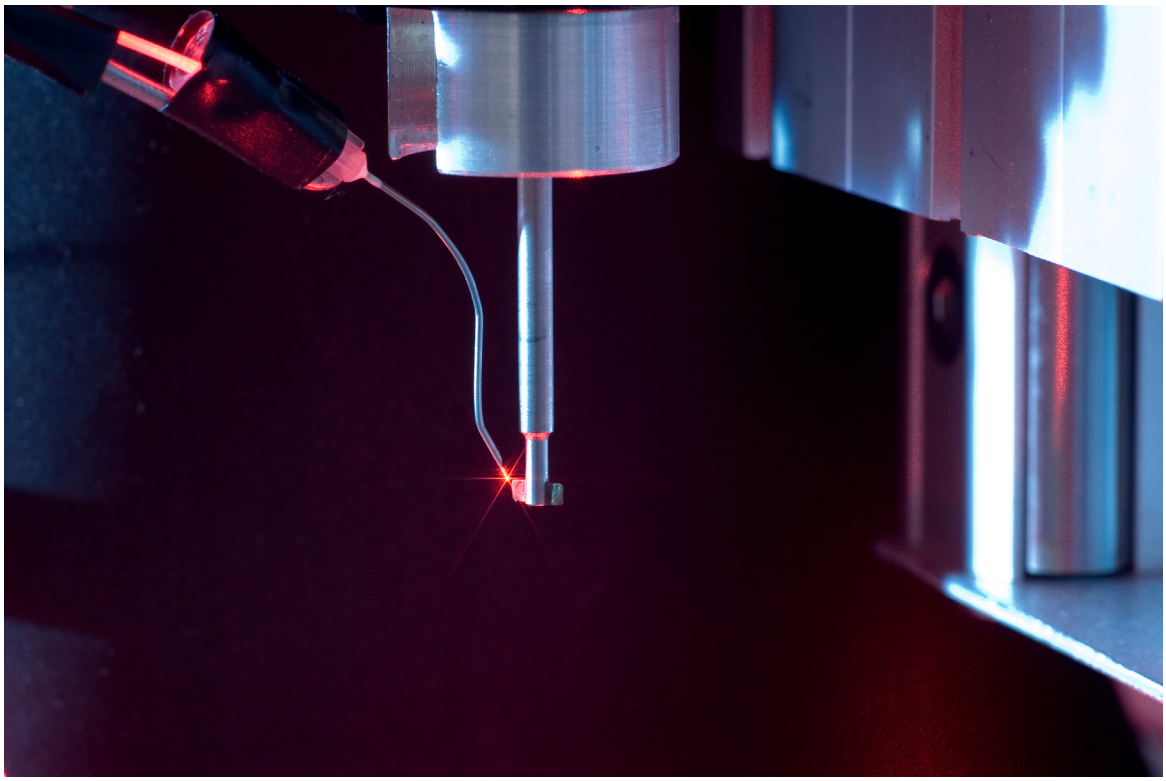

Figure 4: Photograph of the stirring axle with blade and the glass fiber sensor. The sealing cap has been removed in order to allow for dilution experiments (see above). A 23 gauge hollow injection needle replaces the fiber channel. The excitation power at the end of the glass fiber is 2 mW. The plexi glass fluid cell is missing.

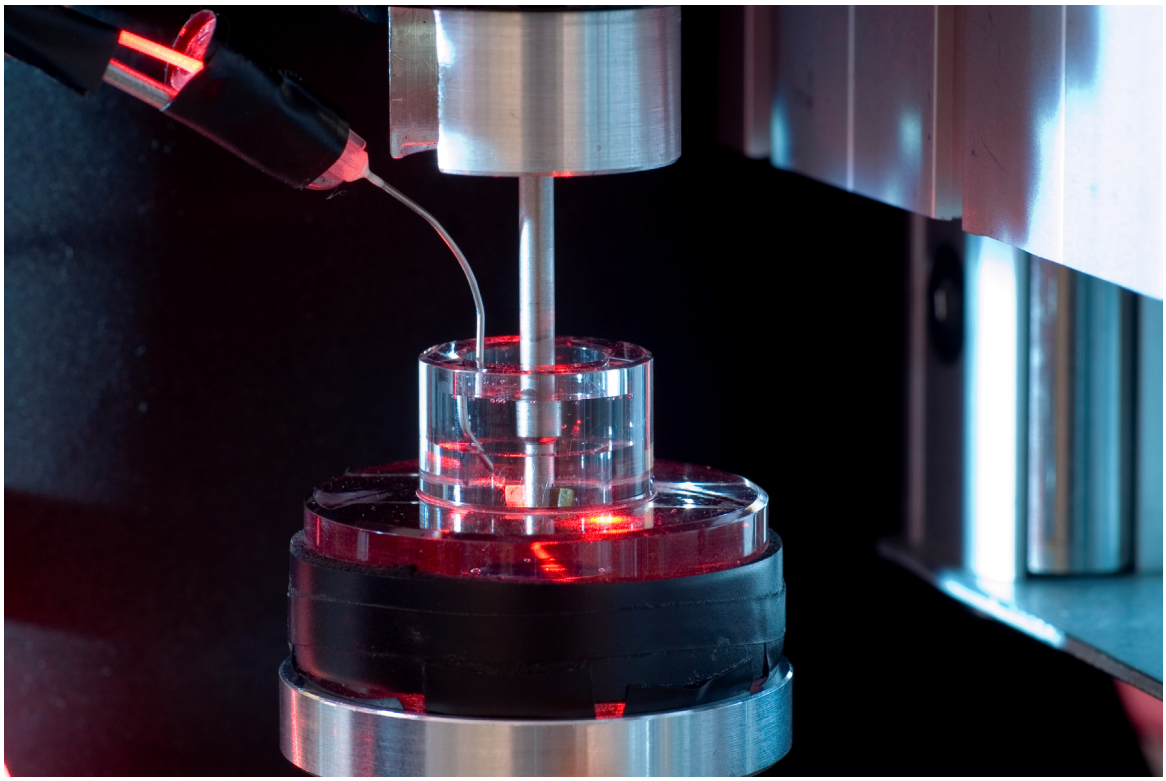

Figure 5: Photograph of the stirring axle with blade and the glass fiber sensor. The sealing cap has been removed in order to allow for dilution experiments (see above). A 23 gauge hollow injection needle replaces the fiber channel. The excitation power at the end of the glass fiber is 2 mW. The plexi glass fluid cell is placed in its apron. This configuration allows to remove and to add sample solution with a pipette under constant stirring. This configuration was applied for measurements that are described in chapters 4, 5 and 6.

9. Acknowledgements

I especially want to thank my doctoral advisor Prof. Dr. Bert Hecht for his outstanding support during this thesis. Without him this work might never have been possible. I will always remember this period of time with great joy. It really was an inspiration and I look forward to many more years of friendship and collaboration.

I also would like to thank Prof. Dr. Hans-Joachim Güntherodt for this extraordinary opportunity of doing my thesis in experimental physics. His vision for the importance of the nanosciences in the field of medicine for the future has strongly influenced my choice of career.

My special thanks go to PD Dr. Martin Hegner, which always made his time available to me for the most inquisitive questions. His guidance and esprit was essential for the realization of this work.

Many thanks also to Dr. Michel Calame who significantly contributed so many useful ideas and suggestions for the molecular beacons. Merci Michel.

Furthermore I would like to thank Dr. Wilfried Grange for his outstanding work on the algorithm for this novel quantification method. Without his programming skills the sensor never would have left the bay.

In addition I would like to mention the very important contribution of Andreas Lieb to the threshold algorithm, another important critical step for the detection method.

Most of all, I do owe many thanks to the workshop of the technical department of the Institute of Physics. Without them, all of this would have remained “theoretical physics”. Heinz Breitenstein, Peter Reimann, Vreni Thommen and especially Silvester Jakob. To all of you, many thanks !

I also owe a lot to Jean-Pierre Ramseier for his strong support. His contributions were very important for the sample holders.

Finally, I would like to express my gratitude for the outstanding support of Dr. med. Andreas Wild. A project like this would never have been possible without such a strong collaboration and friendship. With him the thousands of hours spent in the lab were always fun. Many thanks, bro !

This Dissertation was realized within the NCCR (National Centre for Competence in Research) Nanoscale Sciences.

In addition to the excellent network of the NCCR Nanoscale Sciences made available during this thesis, several additional collaborations were created between the Institute of Physics and the University Hospital of Basel.
Especially the Institute for Pathology and the Department for Ophthalmology have to be mentioned in this context. Their professional support contributed considerably to the success of this project.
I here would like to thank Prof. Dr. med. Michael J. Mihatsch and Prof. Dr. med. Guido Sauter from the Institute of Pathology and Prof. Dr. med. Joseph Flammer from the Department of Ophthalmology for their generous contributions and their professional support.

But most of all I want to thank my wonderful wife, Natalia, who during all these years kept the more mundane things away from me and allowed me to focus on my work. Her support during these inspiring but sometimes challenging times was absolutely decisive. Without you just everything would have been impossible!

10. Patent

(WO/2006/018706) SINGLE ANALYTE MOLECULE DETECTION BY FIBRE FLUORESCENCE PROBE
Latest bibliographic data on file with the International Bureau

Publication No.: WO/2006/018706

International Application No.: PCT/IB2005/002444

Publication Date: 23.02.2006

International Filing Date: 18.08.2005

Int. Class.7: G01N 21/64, G01N 21/77

Applicants:
UNIVERSITY OF BASEL [CH/CH]; Petersgraben 35, WTT-Stelle, CH-4003 Basel (CH).
HECHT, Bert [DE/CH]; Paradiesstrasse 37, CH-4125 Riehen/Basel (CH) *(US Only)*.
HAAS, Philippe [CH/CH]; Spalenring 132, CH-4055 Basel (CH) *(US Only)*.
WILD, Andreas [CH/CH]; Störklingasse 44, CH-4125 Riehen (CH) *(US Only)*.
HEGNER, Martin [CH/CH]; Weizenstrasse 10, CH-4125 Riehen (CH) *(US Only)*.
CALAME, Michel [CH/CH]; Rössligasse 28, CH-4125 Riehen (CH) *(US Only)*.
Inventors:
HECHT, Bert [DE/CH]; Paradiesstrasse 37, CH-4125 Riehen/Basel (CH).
HAAS, Philippe [CH/CH]; Spalenring 132, CH-4055 Basel (CH).
WILD, Andreas [CH/CH]; Störklingasse 44, CH-4125 Riehen (CH).
HEGNER, Martin [CH/CH]; Weizenstrasse 10, CH-4125 Riehen (CH).
CALAME, Michel [CH/CH]; Rössligasse 28, CH-4125 Riehen (CH).
Agent:
UNIVERSITY OF BASEL; Petersgraben 35, WTT-Stelle, CH-4003 Basel (CH).
Priority Data:
60/602,332
18.08.2004
US

Title: SINGLE ANALYTE MOLECULE DETECTION BY FIBRE FLUORESCENCE PROBE

Abstract:

An apparatus for single analyte molecule detection includes: a light source (20) for generating excitation light; a dichroic mirror (22) disposed on a first path of excitation light generated by the light source, wherein the mirror directs excitation light into a fiber aligner (30); an optical transducer coupled to the light source by the fiber aligner, the optical transducer comprising an optical waveguide (40) made of dielectric material having a first dielectrical index; a photon detector (70) disposed to receive fluorescent back radiation, wherein when a test solution having a second dielectric index lower than the first index is provided and comprises one or more target molecules, excitation light is transmitted by the waveguide and exits a waveguide tip disposed in the test solution so as to excite one or more target molecules; subsequently, the waveguide transmits back radiation along a second path to the photon detector that detects the transmitted back radiation.

Designated States:
AE, AG, AL, AM, AT, AU, AZ, BA, BB, BG, BR, BW, BY, BZ, CA, CH, CN, CO, CR, CU, CZ, DE, DK, DM, DZ, EC, EE, EG, ES, FI, GB, GD, GE, GH, GM, HR, HU, ID, IL, IN, IS, JP, KE, KG, KM, KP, KR, KZ, LC, LK, LR, LS, LT, LU, LV, MA, MD, MG, MK, MN, MW, MX, MZ, NA, NG, NI, NO, NZ, OM, PG, PH, PL, PT, RO, RU, SC, SD, SE, SG, SK, SL, SM, SY, TJ, TM, TN, TR, TT, TZ, UA, UG, US, UZ, VC, VN, YU, ZA, ZM, ZW.
African Regional Intellectual Property Org. (ARIPO) (BW, GH, GM, KE, LS, MW, MZ, NA, SD, SL, SZ, TZ, UG, ZM, ZW)
Eurasian Patent Organization (EAPO) (AM, AZ, BY, KG, KZ, MD, RU, TJ, TM)
European Patent Office (EPO) (AT, BE, BG, CH, CY, CZ, DE, DK, EE, ES, FI, FR, GB, GR, HU, IE, IS, IT, LT, LU, LV, MC, NL, PL, PT, RO, SE, SI, SK, TR)
African Intellectual Property Organization (OAPI) (BF, BJ, CF, CG, CI, CM, GA, GN, GQ, GW, ML, MR, NE, SN, TD, TG).

Publication Language: English (EN)

Filing Language: English (EN)